Understanding Transformers for Time Series: Rank Structure, Flow-of-ranks, and Compressibility

Annan Yu,[1,*]   Danielle C. Maddix,[2,†]   Boran Han,[2]   Xiyuan Zhang,[2]

Abdul Fatir Ansari,[2]   Oleksandr Shchur,[2]   Christos Faloutsos,[3]

Andrew Gordon Wilson,[4]   Michael W. Mahoney,[4]   Yuyang Wang[2]

[1] Center for Applied Mathematics, Cornell University, Ithaca, NY 14853, USA
[2] Amazon Web Services (3075 Olcott St, Santa Clara, CA 95054, USA)
[3] Amazon Selling Partner Services (501 Fairview Ave N, Seattle, WA 98109, USA)
[4] Amazon Supply Chain Optimization Technologies (7 West 34th St, New York, NY 10001, USA)

October 7, 2025

Abstract

Transformers are widely used across data modalities, and yet the principles distilled from text models often transfer imperfectly to models trained to other modalities. In this paper, we analyze Transformers through the lens of rank structure. Our focus is on the time series setting, where the structural properties of the data differ remarkably from those of text or vision. We show that time-series embeddings, unlike text or vision, exhibit sharply decaying singular value spectra: small patch sizes and smooth continuous mappings concentrate the data into low-rank subspaces. From this, we prove that the associated $Q/K/V$ projections admit accurate low-rank approximations, and that attention layers become compressible in proportion to the decay of the embedding spectrum. We introduce the concept of *flow-of-ranks*, a phenomenon by which nonlinear mixing across depth inflates the rank, explaining why early layers are most amenable to compression and why ranks grow with depth. Guided by these theoretical and empirical results, we use these insights to compress Chronos, a large time series foundation model, achieving a reduction of 65% in inference time and 81% in memory, without loss of accuracy. Our findings provide principled guidance for allocating width, depth, and heads in time series foundation models, and for exploiting their inherent compressibility.

1 Introduction

Transformers, originally designed for language (Lewis et al., 2020; Achiam et al., 2023), are now widely deployed, e.g., time series (Ansari et al., 2024a; Das et al., 2024; Shi et al., 2025; Wolff et al., 2025), images (Liu et al., 2021; Dosovitskiy et al., 2020), molecules (Maziarka et al., 2020; Leon et al., 2024), and DNA sequences (Ji et al., 2021; Le et al., 2021; Nguyen et al., 2024). A common approach to apply Transformers to these other data modalities is to directly transfer architectural parameters (e.g., width, heads, depth) from text-based models, on the assumption that what works for text should generalize. However, this assumption is fragile. As an example, we show that time series differ fundamentally from language in how signals are tokenized and embedded. This leads to the more general question: how well do community

---

*Work done during an internship at AWS.

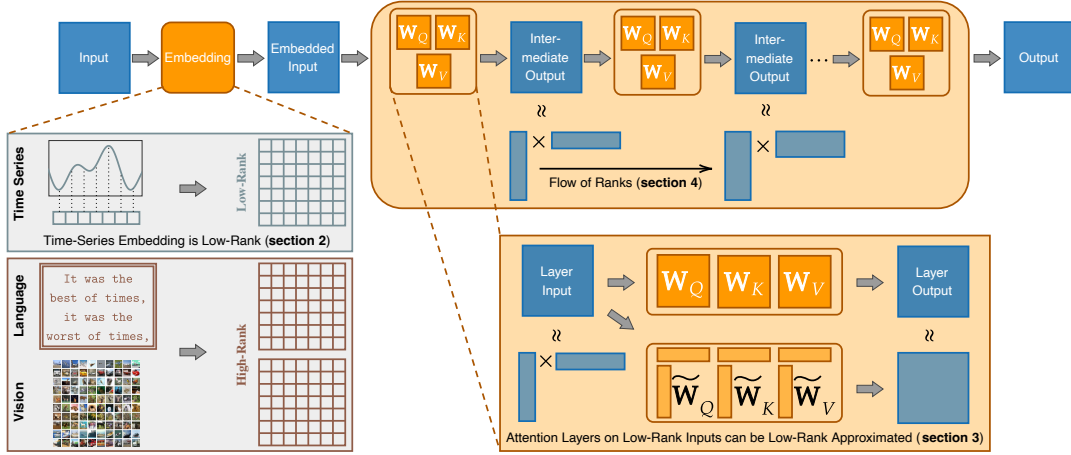†Correspondence to: Danielle C. Maddix <dmmaddix@amazon.com>.

Figure 1: Overview of our results. We show that the embedded inputs of Transformers trained with time-series data have much lower ranks than those of other modalities, including Vision Transformers and Transformers trained with language data (see section 2); we prove that attention matrices on low-rank inputs are well-approximated by low-rank matrices (see section 3); and we introduce and demonstrate a concept called flow-of-ranks, describing how attention matrices in earlier layers are more compressible than those in later layers (see section 4).

insights on pretraining and hyperparameter tuning, based largely on Transformers applied to text data, port to Transformers applied to other data modalities? Understanding the answer to this question is particularly important when Transformers are applied in domains where data are less abundant than in the text domain.

Here, we address this question in the context of time-series data and time-series forecasting. A priori, the answer to this question is not obvious: time series data have similarities with text data (e.g., they have obvious sequential properties), but they also have many differences (e.g., it is not clear that they are well-modelable by a discrete set of tokens). The question, however, is timely: time series data are ubiquitous in many domains, including scientific (Abhishek et al., 2012; Zhang & Gilpin, 2025; Lai et al., 2025), industrial (Hong et al., 2016), and financial applications (Zhang et al., 2001), where they facilitate critical tasks, e.g., forecasting (Hyndman & Athanasopoulos, 2018), imputation (Yoon et al., 2018), and anomaly detection (Blázquez-García et al., 2021). In addition, there has been recent growing interest in developing so-called time series foundation models (TSFMs) (Brown et al., 2020; Radford et al., 2021; Ansari et al., 2024a). These models are large pretrained models, designed with the hope of providing a foundation (Bommasani et al., 2021), to be adaptable to a wide range of domains and time series tasks. As with other models that aim to provide such a "foundation," TSFMs are appealing because they reduce the need for task-specific architectures and parameter computation, thereby enabling the transfer to new settings with relatively little effort.

In this paper, we develop a framework for analyzing design decisions in Transformers; see Figure 1 for an overview and Appendix A for related work. Our view is that these decisions are guided by an understanding of the structural properties of the data modality, which are then inherited by properties of the model. Our framework enables a detailed linear algebraic analysis of the attention layers within a Transformer, which consist of three linear transformations to form the queries, keys, and values. Our approach is general, and we apply it to the time series domain. Lastly, we show that we can use our approach as a practical tool for compressing TSFMs. We summarize the flow of our paper and our main contributions as follows:

1. **Data modality and rank structure.** We compare Transformers trained to different data modalities through the lens of numerical rank, and we demonstrate that time-series data lead

to a particularly low-rank structure, at the level of inputs. To the best of our knowledge, our work is the first to directly study which data modality features make Transformer models well-approximated via a truncated singular value decomposition (SVD), and why. We also show how standard time-series embeddings preserve low-rank structure in the hidden space, which differs from large-vocabulary text and other modalities. (See section 2.)

2. **From low-rank inputs to low-rank attention.** Next, we provide the first general theoretical results that connect low-rank embeddings to low-rank attention matrices, and we make clear how width and the number of heads control the quality of low-rank approximations. While these results apply generally to any low-rank embeddings, we illustrate them in the case of time series. In addition, our results are sharp: we show that high-rank embedded inputs, which appear in data modalities such as text and vision, lead to incompressible attention matrices. (See section 3.)

3. **Flow-of-ranks.** We introduce the "flow-of-ranks" concept to describe how the numerical rank changes across layers in a deep Transformer. This extends our earlier analysis from a single attention layer to the setting of a deep Transformer, where nonlinear activations, residual mixing, and normalization gradually increase the rank of a representation. We note that "flow-of-ranks" explains why early layers are often better approximated by SVD than later ones. (See section 4.)

4. **Compressibility of real-world TSFMs.** Finally, we illustrate one application of our insights: compressing a real-world TSFM. We demonstrate that the same set of hyperparameters (i.e., width, depth, and number of heads) more severely over-parameterizes TSFMs than it does LLMs. This leads us to develop two complementary compression strategies: compressing a pretrained model and pretraining a model that is compressed by design. In particular, we show that by compressing a Chronos model, we can reduce the inference time by 65.4% and memory usage by 81.4%, at no cost of predictive performance. Overall, our results demonstrate and explain why state-of-the-art TSFMs are highly compressible, in practice, compared to (language-trained) LLMs of the same size. (See section 5.)

Additional supporting material may be found in the appendices.

2 Data Modality and Rank Structure of Embedding

In this section, we investigate the structure of time-series embeddings and compare them to embeddings from other data modalities. Our goal is to understand, from both a theoretical and empirical perspective, why time-series inputs often look low-rank after embedding.

We consider univariate time series. In particular, let $\mathbf{x} = (x_1, \ldots, x_T) \in \mathbb{R}^{1 \times T}$ be a univariate input of length T. Note that, unlike other data modalities, the input $\mathbf{x}$ is a rank-1 matrix.[1] The first step in a TSFM is to map $\mathbf{x}$ into a high-dimensional sequence via an embedding function $\mathbf{\Phi} : \mathbb{R}^{1 \times T} \to \mathbb{R}^{d \times L}$, where d denotes the hidden dimension of the model and L denotes the new sequence length, possibly different from T due to patching. This embedding is typically constructed by applying a trainable function $\phi : \mathbb{R}^k \to \mathbb{R}^d$ to disjoint patches of size k. Assuming $L = T/k$ is an integer, this gives:

$$\mathbf{\Phi}(\mathbf{x}) = (\phi(x_1, \ldots, x_k), \phi(x_{k+1}, \ldots, x_{2k}), \ldots, \phi(x_{(L-1)k+1}, \ldots, x_{Lk} = x_T)).$$

These patch embedding functions ϕ fall into two main categories (see Figure 7 in Appendix B):

- A **quantization-based embedding** partitions the input space $\mathbb{R}^k$ into V disjoint regions, $\mathbb{R}^k = \biguplus_{i=1}^{V} R_i$. Each region R_i is mapped to a unique trainable vector $\mathbf{u}_i \in \mathbb{R}^d$, so that

---

[1] In the case of a few-variate time series, $\mathbf{x}$ becomes a few-rank matrix, making the analysis in the paper directly generalizable.

Table 1: Comparison of embedding strategies and patch sizes across TSFMs.

Model	Chronos	WaveToken	TOTEM	Time-MOE	Chronos-Bolt	TimesFM
Strategy	Quantization	Quantization	Quantization	Continuous	Continuous	Continuous
Patch Size	1	1	1	1	16	32

$\phi(\mathbf{x}) = \sum_{i=1}^{V} \mathbb{1}_{\{\mathbf{x} \in R_i\}} \mathbf{u}_i$. This approach is used in several TSFMs, e.g., Chronos (Ansari et al., 2024a), WaveToken (Masserano et al., 2025), and TOTEM (Talukder et al., 2024).

- A **continuous embedding** uses a parameterized function, typically a neural network $\phi(\cdot; \boldsymbol{\theta})$, to map patches directly. This strategy is also used in many TSFMs, e.g., Chronos-Bolt (Ansari et al., 2024b), Moirai (Woo et al., 2024), TimesFM (Das et al., 2024), and Time-MoE (Shi et al., 2025).

Table 1 summarizes the design choices for these prominent TSFMs.

In most TSFMs, the patch size is significantly smaller than the hidden dimension (i.e., $k \ll d$), meaning ϕ maps from a low-dimensional space to a higher-dimensional one. Intuitively, if ϕ is well-behaved, it should embed the low-dimensional space $\mathbb{R}^k$ into a corresponding low-dimensional submanifold $\phi(\mathbb{R}^k) \subset \mathbb{R}^d$. To formalize this notion of dimensionality, we use singular values. Let $\mathbf{U}$ be a linear operator between some Hilbert spaces and $\sigma_1 \geq \cdots \geq \sigma_n \geq 0$ be its singular values, where $1 \leq n \leq \infty$. While the algebraic rank of an object $\mathbf{U}$, i.e., the number of its non-zero singular values, is a strict measure, real-world data is noisy; therefore, we use the more practical concept of numerical rank. For a tolerance $\varepsilon > 0$, the ε-rank of $\mathbf{U}$ denotes the number of its singular values that are significant relative to the largest one:

$$\text{rank}_\varepsilon(\mathbf{U}) = |\{j \mid \sigma_j(\mathbf{U})/\sigma_1(\mathbf{U}) > \varepsilon\}|. \tag{1}$$

A low numerical rank implies $\mathbf{U}$ is well-approximated by an operator $\tilde{\mathbf{U}}$ with $\text{rank}(\tilde{\mathbf{U}}) = \text{rank}_\varepsilon(\mathbf{U})$.

Our central hypothesis is that for a large corpus of input patches $\{\mathbf{x}^{(i)}\}_{i=1}^N$, the resulting embedded matrix, via quantization or a continuous embedding, $\mathbf{U} = \begin{bmatrix} \phi(\mathbf{x}^{(1)}) & \cdots & \phi(\mathbf{x}^{(N)}) \end{bmatrix}$ has a low numerical rank, which is smaller than the ambient dimension d. To test this hypothesis, we sample thousands of patches from diverse signals (e.g., sinusoids, exponential functions, and white noise), and we compute the singular value decay of their embeddings. For contrast, we perform the same analysis on a tabular foundation model (TFM) (Mitra) (Zhang & Robinson, 2025) using 1000 synthetic tables, a T5 LLM processing text from Dickens' *A Tale of Two Cities*, and a ViT processing 1000 randomly sampled images from CIFAR-10.
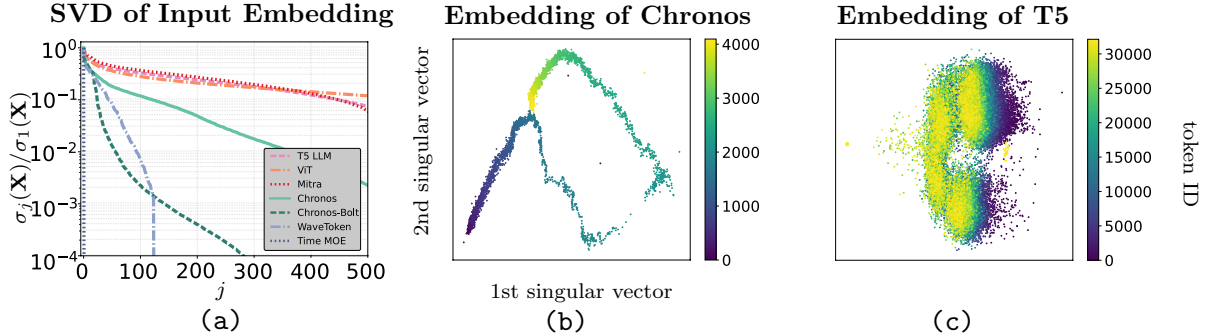

Figure 2: (a): Singular values of the embedded input matrices from many different TSFMs, a TFM, a ViT, and an LLM. (b,c): Embedding space of Chronos and a T5 LLM, respectively, visualized by projecting them onto the leading two singular vectors of the embedding matrix.

As shown in Figure 2(a), the singular values of TSFM embeddings decay dramatically faster

than those from the tabular and language models, which confirms their significantly lower numerical rank. Figure 2(b,c) visualize the embedding spaces of Chronos (quantized) and T5 (language tokens) by projecting them onto their top two singular vectors. The Chronos embedding, mapping a quantized real line, reveals a clear low-dimensional structure, whereas the T5 embedding, likely due to its vocabulary properties, appears far less well-structured.

One may wonder: why is it that Chronos-Bolt ($k = 16$) produces a lower-rank embedding than Chronos ($k = 1$)? This seeming surprise arises from their different embedding mechanisms. A quantization-based model like Chronos initially maps adjacent values to random, unstructured vectors; it must learn the geometry of the real line during training. In contrast, a continuous embedding like Chronos-Bolt uses a smooth neural network $\phi(\cdot; \boldsymbol{\theta})$. This architectural choice imposes smoothness from the start, ensuring that even a randomly initialized model maps the low-dimensional patch space $\mathbb{R}^k$ to a low-dimensional submanifold in $\mathbb{R}^d$ (see Appendix C).

Although understanding a quantization-based embedding requires looking into the training dynamics, which is beyond the scope of this paper, we theoretically analyze how a continuous embedding preserves low-rank structures. The following theorem formalizes this intuition.

Theorem 1. Given any hidden dimension $d > 1$, let $\boldsymbol{\phi} : [-1, 1] \to \mathbb{R}^d$ be a function that embeds $[-1, 1]$ into $\mathbb{R}^d$. Given L arbitrary points $x_1, \ldots, x_L$ sampled from $[-1, 1]$, define

$$\boldsymbol{\Xi} = \begin{bmatrix} - & \phi_1(x) & - \\ & \vdots & \\ - & \phi_d(x) & - \end{bmatrix} \in \mathbb{R}^{d \times [-1,1]}, \qquad \boldsymbol{\Psi} = \begin{bmatrix} \phi_1(x_1) & \cdots & \phi_1(x_L) \\ \vdots & \ddots & \vdots \\ \phi_d(x_1) & \cdots & \phi_d(x_L) \end{bmatrix} \in \mathbb{R}^{d \times L}.$$

Let $s_1 \geq \cdots \geq s_d \geq 0$ and $\sigma_1 \geq \cdots \geq \sigma_d \geq 0$ be the singular values of the quasimatrix $\boldsymbol{\Xi}$ and matrix $\boldsymbol{\Psi}$, respectively. Then, the following statement holds:

1. If, for some $V > 0$, $\nu \geq 1$, and every $1 \leq i \leq d$, we have ϕ_i and its derivative through $\phi_i^{(\nu)}$ are absolutely continuous on $[-1, 1]$ and $\phi_i^{(\nu)}$ is of bounded variation V, then we have

$$s_{j+1} \leq \frac{4V\sqrt{d}}{\pi\nu(j-1-\nu)^\nu} = \mathcal{O}(j^{-\nu}\sqrt{d}), \quad \sigma_{j+1} \leq \frac{2V\sqrt{dL}}{\pi\nu(j-1-\nu)^\nu} = \mathcal{O}(j^{-\nu}\sqrt{dL}), \quad \nu+1 < j \leq d-1.$$

2. If, for some $M > 0$ and every $1 \leq i \leq d$, ϕ_i has an analytic continuation to the Bernstein ellipse of radius $\rho > 1$ (see Trefethen (2019)), whose infinity norm is no greater than M, then we have

$$s_{j+1} \leq \frac{4M\sqrt{d}\rho^{-j+1}}{\rho - 1} = \mathcal{O}(\rho^{-j}\sqrt{d}), \quad \sigma_{j+1} \leq \frac{2M\sqrt{dL}\rho^{-j+1}}{\rho - 1} = \mathcal{O}(\rho^{-j}\sqrt{dL}), \quad 0 \leq j \leq d-1.$$

We refer interested readers to Townsend & Trefethen (2015) for the precise definition of a quasimatrix (informally, it is a "matrix" in which one of the dimensions is discrete as usual but the other is continuous). Theorem 1 guarantees that for univariate patches ($k = 1$), a smooth embedding function yields singular values with guaranteed decay rates: polynomial decay of order ν for functions with ν continuous derivatives, and exponential decay for analytic functions.

See Appendix B for a proof of Theorem 1 using classic univariate polynomial approximation techniques. Using this result, we can directly explain the low-rank structure observed in models like Time-MoE (see Figure 2 and Corollary 2). While multivariate polynomial approximation results enable us to extend Theorem 1, the size of the polynomial basis up to a fixed degree increases exponentially with k, which makes it less practically relevant for a larger patch size k. Instead, for Chronos-Bolt, where $k = 16$, we seek an ad hoc result that works when the embedding $\phi(\cdot; \boldsymbol{\theta})$ is an MLP (see Appendix D for a proof of Theorem 2 below).

Theorem 2. Consider the input embedding defined by a two-layer residual MLP:

$$\mathbf{\Phi}(\mathbf{X}) = \mathbf{W}_3\mathbf{X} + \mathbf{W}_2\,\omega(\mathbf{W}_1\mathbf{X}), \quad \mathbf{X} \in \mathbb{R}^{k \times L}, \quad \mathbf{W}_1 \in \mathbb{R}^{d_f \times k}, \quad \mathbf{W}_2 \in \mathbb{R}^{d \times d_f}, \quad \mathbf{W}_3 \in \mathbb{R}^{d \times k},$$

where k denotes the patch size, L denotes the number of patches, d_f denotes the hidden-layer dimension in an MLP, $d > k$ denotes the hidden dimension of the Transformer, and ω denotes any activation function satisfying that $|\omega(x)| \leq |x|$ for every $x \in \mathbb{R}$. Then, for any $\varepsilon > 0$, we have

$$|\{j \mid \sigma_j(\mathbf{\Phi}(\mathbf{X})) > \varepsilon \|\mathbf{W}_2\|_2 \|\mathbf{W}_1\mathbf{X}\|_2\}| \leq (1 + \varepsilon^{-2})k.$$

Theorem 2 states that the numerical rank of the continuous embedding is bounded by a quantity dependent on the patch size k, not the much larger ambient dimension d. The term $\|\mathbf{W}_2\|_2 \|\mathbf{W}_1\mathbf{X}\|_2$ reflects the natural scaling of $\sigma_1(\mathbf{\Phi}(\mathbf{X}))$ that appears in the definition of rank_ε. In practice, we have $k \ll d$, meaning that MLP embeds an input patch in $\mathbb{R}^k$ into a low-dimensional subspace in $\mathbb{R}^d$.

To illustrate this theorem, we pretrain 6 Chronos-Bolt models of different patch sizes, and we compute the singular values of their embeddings. Figure 3(a) shows that the numerical rank of the embedding increases with the patch size k. We also perform an in-depth analysis, where for each pair of embedded inputs $\phi(\mathbf{x}^{(i)})$ and $\phi(\mathbf{x}^{(j)}) \in \mathbb{R}^d$, we compute the angle between them as follows:

$$\theta(\phi(\mathbf{x}^{(i)}), \phi(\mathbf{x}^{(j)})) = |\phi(\mathbf{x}^{(i)})^\top \phi(\mathbf{x}^{(j)})| / (\|\phi(\mathbf{x}^{(i)})\|_2 \|\phi(\mathbf{x}^{(j)})\|_2) \in [0, \pi/2]. \tag{2}$$

The larger the θ, the more linearly independent the two vectors are. We illustrate this in Figure 3(b), where brighter the heatmaps correspond to higher rank matrices. We see that the embedded input, $\mathbf{\Phi}(\mathbf{X})$ from Chronos-Bolt, which is a subset of $\mathbb{R}^d = \mathbb{R}^{768}$, spans a subspace of significantly smaller dimension, i.e., the image of $\mathbb{R}^k = \mathbb{R}^{16}$ under ϕ.
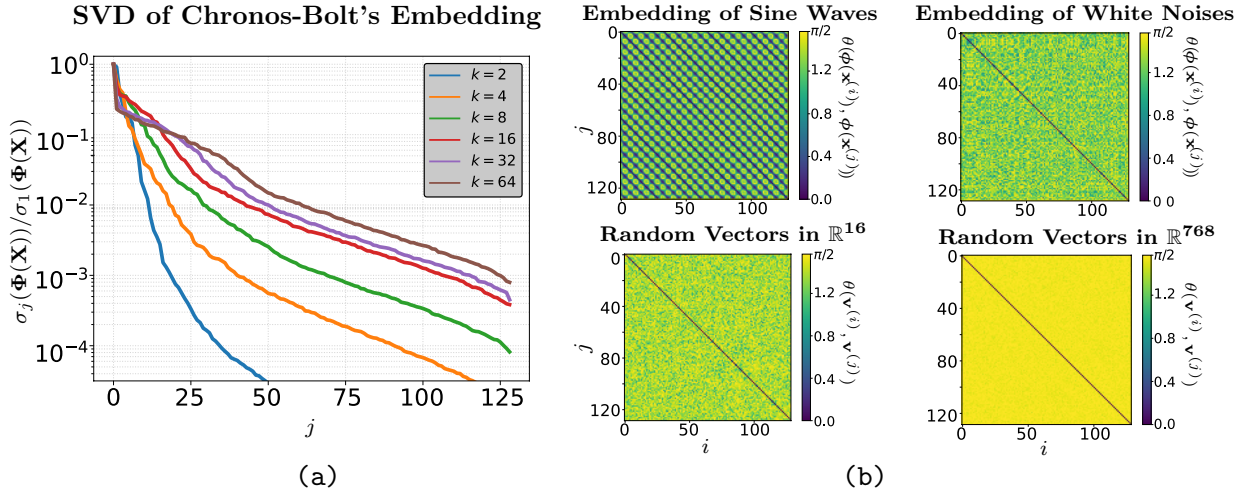

Figure 3: (a): Singular values of the embedded input matrices from Chronos-Bolt models pretrained with different patch sizes k. (b): Angles between Chronos-Bolt's embedded vectors in $\mathbb{R}^d = \mathbb{R}^{768}$ defined in eq. (2), where the patches $\mathbf{x}^{(i)}$ are from a sinusoidal wave and Gaussian white noises, respectively. We also plot the angles between i.i.d. random Gaussian vectors in $\mathbb{R}^k = \mathbb{R}^{16}$ and $\mathbb{R}^d = \mathbb{R}^{768}$ for comparison.

3 From Low-rank Inputs to Low-rank Attention Matrices

Let $\mathbf{U} \in \mathbb{R}^{d \times L}$ be an input embedded in the hidden space. Recall that in section 2 we showed that for TSFMs, $\mathbf{U}$ often has a low numerical rank. This immediately implies $\mathbf{U}$ can be expressed in a low-rank format: $\mathbf{U} \approx \mathbf{U}_1\mathbf{U}_2$, where $\mathbf{U}_1 \in \mathbb{R}^{d \times \tilde{d}}$ and $\mathbf{U}_2 \in \mathbb{R}^{\tilde{d} \times L}$ for some $\tilde{d} \ll d$. This yields

faster matrix-matrix products with $\mathbf{U}$, but a limitation is that this representation requires an expensive rank-revealing matrix factorization (Damle et al., 2024), which adds overhead, particularly during backpropagation. If so, how do we leverage the low-rank structure of TSFM embeddings?

From basic linear algebra, it is known that for a linear operator $\mathbf{T} : \mathbb{R}^d \rightarrow \mathbb{R}^d$ to act on an r-dimensional subspace, one only needs to specify the operator in r directions, in which case the operator can then be well-approximated by a low-rank matrix $\tilde{\mathbf{T}}$ whose rank scales with r instead of the full width d (Damle et al., 2024; Ipsen & Saibaba, 2024). An attention layer, defined by

$$\text{Attention}(\mathbf{U}; \mathbf{W}_Q, \mathbf{W}_K, \mathbf{W}_V) = \mathbf{W}_V \mathbf{U} \, \text{softmax}\left(\frac{\mathbf{U}^\top \mathbf{W}_Q^\top \mathbf{W}_K^\top \mathbf{U}}{\sqrt{d}}\right), \quad \mathbf{W}_Q, \mathbf{W}_K, \mathbf{W}_V \in \mathbb{R}^{d \times d},$$

while nonlinear, contains three linear transformations: namely, the queries, the keys, and the values. In this section, we establish Theorem 3, which supports the low-rank representations of $\mathbf{W}_Q$, $\mathbf{W}_K$, and $\mathbf{W}_V$ given a low-rank $\mathbf{U}$ (see Appendix E for the proof).

Theorem 3. Let $C > 0$ be a constant. Let $\boldsymbol{\Xi} = \begin{bmatrix} \mathbf{x}_1 & \cdots & \mathbf{x}_N \end{bmatrix} \in \mathbb{R}^{d \times N}$ be given for some $d, N \geq 1$, $\mathbf{x}_j \in \mathbb{R}^d$, and $\|\mathbf{x}_j\|_2 \leq C$ for all $1 \leq j \leq N$. Let $\mathbf{W}_Q, \mathbf{W}_K, \mathbf{W}_V \in \mathbb{R}^{d \times d}$ be matrices such that $\|\mathbf{W}_Q^\top \mathbf{W}_K\|_2 \leq C\sqrt{d}$, and $\|\mathbf{W}_V\|_2 \leq C\sqrt{d}$. The following two statements hold:

1. **(Attention matrices are compressible on low-rank inputs.)** For any $\tilde{d} < d$ such that $\sigma_{\tilde{d}+1} := \sigma_{\tilde{d}+1}(\boldsymbol{\Xi}) \leq 1$, there exist $\tilde{\mathbf{W}}_Q, \tilde{\mathbf{W}}_K, \tilde{\mathbf{W}}_V \in \mathbb{R}^{d \times d}$ with $\text{rank}(\tilde{\mathbf{W}}_Q) = \text{rank}(\tilde{\mathbf{W}}_K) = \text{rank}(\tilde{\mathbf{W}}_V) = \tilde{d}$, $\|\tilde{\mathbf{W}}_Q^\top \tilde{\mathbf{W}}_K\|_2 \leq \|\mathbf{W}_Q^\top \mathbf{W}_K\|_2$, and $\|\tilde{\mathbf{W}}_V\|_2 \leq \|\mathbf{W}_V\|_2$, such that given any matrix $\mathbf{U} \in \mathbb{R}^{d \times L}$ for any $L \geq 1$, where each column of $\mathbf{U}$ is a column of $\boldsymbol{\Xi}$, we have that

$$\left\| \text{Attention}(\mathbf{U}; \mathbf{W}_Q, \mathbf{W}_K, \mathbf{W}_V) - \text{Attention}(\mathbf{U}; \tilde{\mathbf{W}}_Q, \tilde{\mathbf{W}}_K, \tilde{\mathbf{W}}_V) \right\|_F \leq \mathcal{O}\left(\sqrt{d}\,\sigma_{\tilde{d}+1}\right), \quad (3)$$

where the constant in the $\mathcal{O}$-notation only depends on C.

2. **(Attention matrices are incompressible on high-rank inputs.)** The upper bound in eq. (3) is tight up to a factor of $\sqrt{d}$. That is, fix some $d \geq 1$, $L \geq d$, and a sequence $1 \geq \sigma_1 \geq \sigma_2 \geq \cdots \geq \sigma_d > 0$. There exist $\mathbf{U} \in \mathbb{R}^{d \times L}$ with $\sigma_j(\mathbf{U}) = \sigma_j$ for all $1 \leq j \leq d$, and $\mathbf{W}_Q, \mathbf{W}_K \in \mathbb{R}^{d \times d}$ such that for any $\tilde{d} < d$, any orthogonal matrix $\mathbf{W}_V \in \mathbb{R}^{d \times d}$, and any rank-$\tilde{d}$ matrix $\tilde{\mathbf{W}}_V \in \mathbb{R}^{d \times d}$, we have

$$\left\| \text{Attention}(\mathbf{U}; \mathbf{W}_Q, \mathbf{W}_K, \mathbf{W}_V) - \text{Attention}(\mathbf{U}; \mathbf{W}_Q, \mathbf{W}_K, \tilde{\mathbf{W}}_V) \right\|_F \geq \frac{1}{4}\sigma_{\tilde{d}+1}. \quad (4)$$

The first statement of Theorem 3 says, at a high level, that if the inputs $\mathbf{U}$ come from a low-rank vocabulary $\boldsymbol{\Xi}$, i.e., $\sigma_{\tilde{d}+1}$ is small, then one only needs low-rank attention matrices $\tilde{\mathbf{W}}_Q, \tilde{\mathbf{W}}_K, \tilde{\mathbf{W}}_V$ on $\mathbf{U}$. Here, it is important that we fix the low-rank embedded space $\boldsymbol{\Xi}$ and prove a uniform bound eq. (3) that holds for all input $\mathbf{U}$, so that our low-rank approximation $\tilde{\mathbf{W}}_Q, \tilde{\mathbf{W}}_K, \tilde{\mathbf{W}}_V$ is not input-dependent. Since TSFMs have a low-rank vocabulary $\boldsymbol{\Xi}$ (see section 2), high-rank attention matrices in TSFMs can be approximated by low-rank ones. See Appendix F for a numerical experiment.

For other data modalities than time-series, e.g., TFMs, ViTs, and LLMs (see Figure 2), where $\mathbf{U}$ has a higher rank, the second statement of Theorem 3 suggests that the attention matrices are less compressible, as we will show in section 5.

To illustrate the concepts in Theorem 3 on TSFMs, we take pretrained Chronos models and T5 LLMs of different hidden dimensions d. These two models have the same Transformer size and architecture, and differ only in the pretraining data modality. For each model and a fixed $\varepsilon > 0$, we compute the averaged ε-rank of all query projection matrices $\mathbf{W}_Q$ from the model.

Figure 4(a,b) show that as the size of $\mathbf{W}_Q$ increases, the matrix $\mathbf{W}_Q$ stays low-rank in a Chronos model, and its rank scales almost linearly with d in a T5 LLM. For Chronos models, where the vocabulary is embedded in a low-rank subspace, low-rank attention matrices suffice to capture most information in the inputs. This empirical observation goes beyond Theorem 3, which proves the sufficiency of low-rank $\mathbf{W}_{Q/K/V}$, but it does not guarantee their appearance via training. Figure 4(a) shows that training, while independent from expressiveness, gives rise to low-rank weights (see Appendix G for more insights). This provides motivation for pretraining a compressed model and for compressing a pretrained one (see section 5). In Appendix G, we show an analysis of the distribution of the singular values of attention matrices, in pretrained foundation models and also during training.
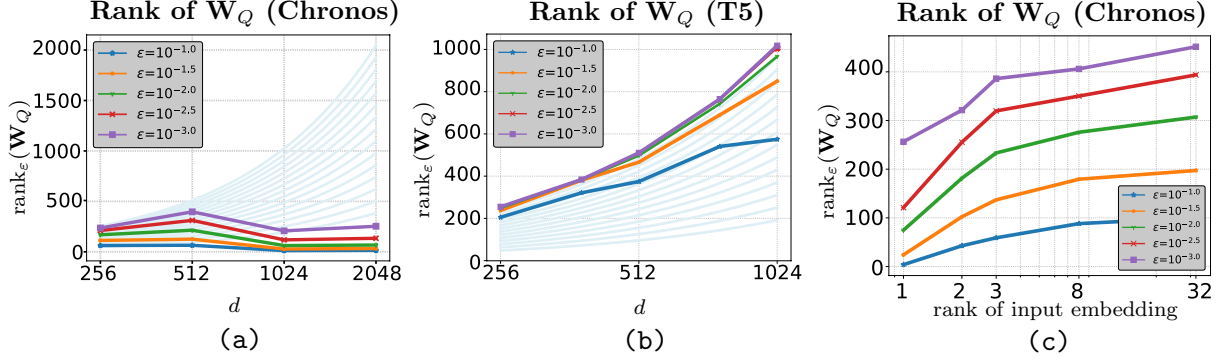

Figure 4: The averaged ε-rank of query projection matrices $\mathbf{W}_Q$ in pretrained Chronos models and T5 LLMs. In (a,b), we vary the hidden dimension d. The light blue curves are contours of the ratio between the horizontal and the vertical axes in the semilog-x scale. In (c), we fix the hidden dimension $d = 512$ and change the rank of the fixed input embedding $\mathbf{\Xi}$ (see Appendix H).

To further corroborate the role of the rank $\tilde{d}$ in Theorem 3, we pretrain Chronos models with a fixed vocabulary. We increase the (algebraic) rank of $\mathbf{\Xi}$ from 1 to 32 (see Appendix H), where we observe that the numerical ranks of attention matrices increase with rank($\mathbf{\Xi}$) (see Figure 4(c)).

While our discussion in this section assumes a single head in the attention layer, in Appendix I we extend the result to the multi-head case. From the standpoint of representation complexity, Theorem 3 applies equally to multi-head attention, and it is independent of the number of heads (see Theorem 5 in Appendix E). In practice, however, we observe that the $\mathbf{W}_{Q/K/V}$ matrices in pretrained multi-head layers tend to have higher numerical ranks (see Figure 16). This effect can be understood through the lens of numerical linear algebra, via a concept called "sketching" (see Appendix I). It helps explain why additional heads can improve robustness and training stability, even though the underlying complexity result is head-agnostic (see Theorem 6 in Appendix I).

4 Flow-of-ranks: Moving through a Transformer

Our prior discussions in section 3 focused on compressing a single attention layer, but a Transformer in a TSFM has many layers. While we showed that the input into the first attention layer is low-rank (see section 2), one may wonder: what about the inputs into a later layer? If you apply a linear transformation to a low-rank input, then it at most preserves, if not decreases, the rank of the input; however, each layer in a Transformer is generally nonlinear. Here, we demonstrate that these nonlinear layers can increase the rank of the input.

We refer to the phenomenon of the increasing rank of the input as it goes deeper into the layers of a model as the *flow-of-ranks*. Our contribution here is twofold: we quantify this rank growth across layers in a deep Transformer by proving Theorem 4 and then show what that

means to Transformers applied to time-series data. To see the "flow-of-ranks" in practice, we show the numerical ranks of attention matrices per layer in a Chronos model and a T5 LLM in Figure 5(a,b). The numerical ranks of attention matrices become higher for deeper layers because of the flow-of-ranks (see Figure 5(c)). For a T5 LLM, only with a large ε do we observe an increase in the ε-rank, because the ε-rank with a small ε is already saturated (i.e., close to the matrix's dimension) to capture the high-rank vocabulary $\mathbf{\Xi}$. To formalize this discussion, we prove how an attention layer increases the small singular values of a low-rank input matrix.

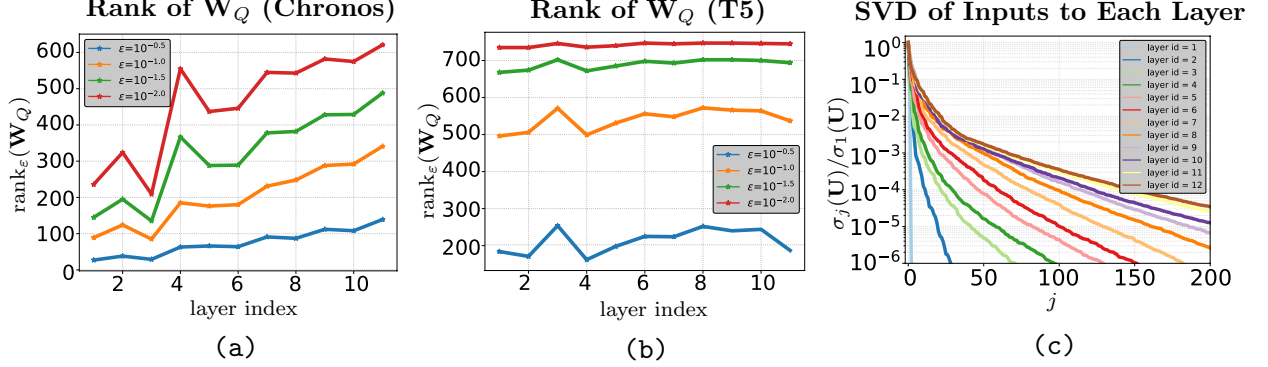**Figure 5:** (a,b): The ε-rank of every query projection $\mathbf{W}_Q$ in the encoder of a Chronos model and a T5 model of the same size, respectively. (c): Singular values of the input matrix to each Chronos' encoder layer, starting with a constant signal $(x_1, \ldots, x_T) = (0, \ldots, 0)$.

Theorem 4. Given positive integers $d \leq L$, let $\mathbf{U} \in \mathbb{R}^{d \times L}$ be an input matrix with singular values $1 = \sigma_1 \geq \cdots \geq \sigma_d > 0$. Let $D \geq 1$ be the number of layers of the model. Let h be the number of heads and d_h be the per-head dimension so that $d = h \times d_h$. The following statements hold:

1. Suppose $\sqrt{D} \geq 2e^2h$. For every $1 \leq i \leq h$, let $\|\mathbf{W}_Q^{(i)\top}\mathbf{W}_K^{(i)}\|_2 \leq \sqrt{d_h}$, and $\|\mathbf{W}_V^{(i)}\|_2 \leq 1$ be any attention matrices (see eq. (19) for the notation). For any $1 \leq k \leq d$, we have

$$\sigma_k(\mathbf{Z})/\sigma_1(\mathbf{Z}) \leq 2 \min_{1 \leq j \leq k} \left(\sigma_{k-j+1} + \frac{e^2 h}{\sqrt{D}} \sigma_{\lfloor (j-1)/h \rfloor + 1} \right), \tag{5}$$

where $\mathbf{Z} = \mathbf{U} + \mathbf{Y}/\sqrt{D}$ and $\mathbf{Y} = \text{MH-Attention}(\mathbf{U}; \mathbf{W}_Q, \mathbf{W}_K, \mathbf{W}_V, h)$.

2. The upper bound above is tight. More precisely, given any d, L, N, h, and singular values $1 = \sigma_1 \geq \cdots \geq \sigma_d > 0$, there exist an input $\mathbf{U} \in \mathbb{R}^{d \times L}$ with singular values $\sigma_1, \ldots, \sigma_d$, and matrices $\mathbf{W}_Q$, $\mathbf{W}_K$, and $\mathbf{W}_V$ with $\|\mathbf{W}_V^{(i)}\|_2 \leq 1$, such that for any $1 \leq k \leq d$, we have

$$\sigma_k(\mathbf{Z})/\sigma_1(\mathbf{Z}) \geq \frac{1}{4} \left(\sigma_{(i-1)d_h + \lceil k/i \rceil} + \frac{1}{\sqrt{D}} \sigma_{\lceil k/i \rceil} \right), \tag{6}$$

for every $i \leq h$ such that $\lceil k/i \rceil < d_h$.

See Appendix J for the proof of Theorem 4 and Appendix F for a numerical experiment. The matrix $\mathbf{Z}$ can be interpreted as the output of a residual attention layer given input $\mathbf{U}$, where the scaling factor $1/\sqrt{D}$ is commonly used in a Transformer to stabilize and accelerate training (De & Smith, 2020). The upper bound in eq. (5) provides a guarantee that the rank of the output cannot be arbitrarily large if the input is low-rank. In this bound, there are two terms balancing each other: σ_{k-j+1}, which increases as j increases, and $\sigma_{\lfloor (j-1)/h \rfloor + 1}$, which decreases as j increases. Without knowing the precise distribution of the singular values, the j which minimizes eq. (5) cannot be determined. To understand why the upper bound is tight, we prove a corollary in a simplified one-layer setting.

Corollary 1. Using the notations in Theorem 4 and assuming $D = 1$, we have $\sigma_k(\mathbf{Z}) \leq \mathcal{O}(h)\sigma_{\lfloor (k+1)/(h+1) \rfloor + 1}$. In addition, the lower bound eq. (6) satisfies that $\sigma_k(\mathbf{Z}) \geq \mathcal{O}(1)\sigma_{\lceil k/h \rceil}$ for every $k \leq d - d_h$. The constants in both $\mathcal{O}$-notations are universal.

The corollary states that when $\mathbf{U}$ goes through an attention layer, the kth singular value of the output $\mathbf{Z}$ can be increased to at most the order of magnitude of the $\lfloor k/h \rfloor^{\text{th}}$ singular value of $\mathbf{U}$. The lower bound suggests that this can be achieved by some inputs, which proves the sharpness of the upper bound. Interestingly, this result says that the number of heads h plays an important role in increasing the ranks of an input matrix. The term to note here is not the $\mathcal{O}(h)$ factor multiplied to the upper bound but the division by $h + 1$ in the subindex $\lfloor (k+1)/(h+1) \rfloor + 1$. When h is large and the singular values decay fast, $\sigma_{\lfloor (k+1)/(h+1) \rfloor + 1}(\mathbf{U})$ can be significantly larger than $\sigma_k(\mathbf{U})$ (see Figure 11).

5 Using these insights: How to Compress a TSFM?

In this section, we apply our theoretical framework to compress large TSFMs. We pursue two approaches: first, motivated by the observation that attention matrices in many pretrained TSFMs are already low rank, we apply truncated SVD to each attention matrix of a pretrained model. Second, to achieve stronger compression, we design architectures that parameterize attention matrices in low rank from the start and pretrain them from scratch, using a layer-dependent hyperparameter schedule that accounts for the "flow-of-ranks." We present results on compressing Chronos, and we provide more results on another TSFM in Appendix K to support the broad applicability of our methods.

Compressing a Pretrained Model. In Figure 4, we see that attention matrices in a large pretrained model usually do not have a full numerical rank. That means we can well-approximate a large matrix with a low-rank one. More precisely, let $\mathbf{W} \in \mathbb{R}^{d \times d}$ be an attention matrix and let $\mathbf{W} = \sum_{j=1}^{d} \sigma_j \mathbf{u}_i \mathbf{v}_i^\top$ be the singular value decomposition (SVD) of $\mathbf{W}$. Then, for a fixed $\varepsilon > 0$, the truncated SVD satisfies a relative error bound: $\left\| \mathbf{W} - \sum_{j=1}^{\text{rank}_\varepsilon(\mathbf{W})} \sigma_j \mathbf{u}_i \mathbf{v}_i^\top \right\|_2 \leq \varepsilon \|\mathbf{W}\|_2$ (see eq. (1)). For a fixed $\varepsilon > 0$, we apply the truncated SVD to every attention matrix of the pretrained Chronos model without fine-tuning, which reduces the number of parameters. We compute the WQL and MASE losses (see Ansari et al. (2024a)) and their geometric means relative to the original model. A score below 1 means the reduced model performs better while it performs worse otherwise.

Table 2: Results of compressing a pretrained Chronos or T5 model. We apply truncated SVD with a specific ε, which results in a model whose attention matrices are compressed to the "Ratio" of the original size. We compare the performance scores relative to the original pretrained model, where "LPPL" stands for the logarithm of the perplexity. Overlap is obtained by selecting the top-10 tokens from the original model and the compressed one, and computing their Jaccard overlap.

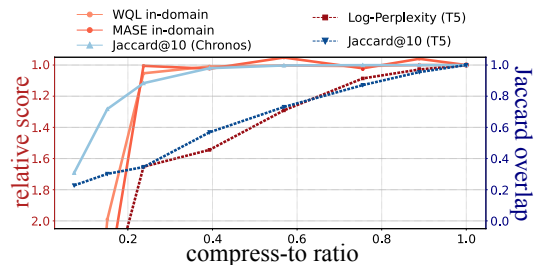| Ratio | Chronos | | | | | T5 | |
| | In-Domain ↓ | | Zero-Shot ↓ | | Overlap ↑ | LPPL ↓ | Overlap ↑ |
	WQL	MASE	WQL	MASE			
0.073	4.409	4.095	3.562	3.435	0.308	3.313	0.227
0.151	1.991	2.412	1.566	1.576	0.717	2.530	0.301
0.237	1.053	1.005	1.030	1.011	0.883	1.652	0.345
0.393	1.009	1.024	0.990	0.994	0.979	1.544	0.568
0.569	1.003	0.952	0.945	0.995	0.997	1.290	0.730
0.755	1.007	1.021	1.027	1.000	0.999	1.085	0.871
0.889	1.000	0.960	1.016	1.001	0.999	1.028	0.954
1.000	1.000	1.000	1.000	1.000	1.000	1.000	1.000

Table 2 shows that we can compress the attention matrices up to around 23.7% of the original size without any loss of performance. Reducing the size further takes away key information in attention matrices and results in a rapid performance deterioration, leading us to the next compression method.

Pretraining a Compressed Model. Table 2 shows a hard limit of compression: compressing

the size to below about 20% makes the performance significantly worse. If one is given enough budget, a more robust method to obtain a smaller TSFM is by pretraining a compressed model. We parameterize a $d \times d$ attention matrix by a rank-$\tilde{d}$ representation. Driven by "flow-of-ranks" from section 4, we choose to let $\tilde{d}$ be layer-dependent. In the ith layer of the model, we use a $\tilde{d}_i = \tilde{d}(i) = \lceil \tilde{d}_0(1+i)^\alpha \rceil$, where $\tilde{d}_0 > 0$ and $\alpha \geq 0$ are two hyperparameters. This design is motivated by the fact that the numerical rank of an input to a layer increases as the layer index, and we need attention matrices of higher ranks to capture them (see Theorem 3). In Figure 6, we see how pretraining a compressed model allows us to expand the time–accuracy Pareto frontier of TSFMs, where numerical accuracies can be found in Table 3, which show that pretraining a compressed model is more robust than compressing a pretrained one. In fact, in Table 4 of Appendix K, we show that pretraining a compressed Chronos-Bolt allows us to outperform even traditional local methods on *both* time and accuracy.
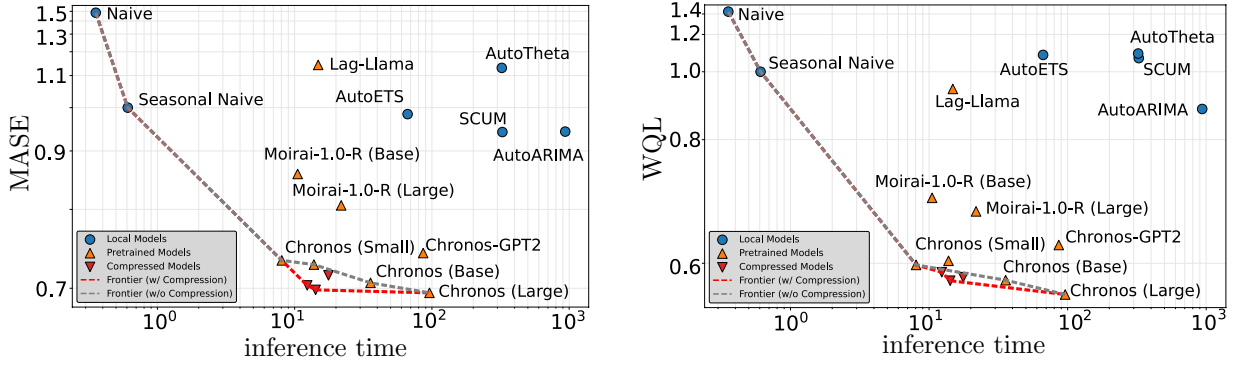

Figure 6: Results of pretraining a compressed Chronos model. These results show how pre-training the compressed Chronos model expands the Pareto frontier of time-series modeling. See Table 3 for more data and results.

6   Conclusion

We have developed a data/modality-dependent framework via the lens of rank structure for analyzing the structure of and design decisions for Transformers, and we have applied it to Chronos and Chronos-Bolt, two popular TSFMs. Our results highlight how properties of the model depend on and interact with properties of the input data, and they lead to concrete principles for the design of models, parameters, and hyperparameters. We illustrate our proof-of-principle results by showing the compressibility of Chronos and Chronos-Bolt in comparison to Transformers trained on text data.

Acknowledgments

References

Kumar Abhishek, Maheshwari Prasad Singh, Saswata Ghosh, and Abhishek Anand. Weather forecasting model using artificial neural network. *Procedia Technology*, 4:311–318, 2012.

Josh Achiam, Steven Adler, Sandhini Agarwal, Lama Ahmad, Ilge Akkaya, Florencia Leoni Aleman, Diogo Almeida, Janko Altenschmidt, Sam Altman, Shyamal Anadkat, et al. Gpt-4 technical report. *arXiv preprint arXiv:2303.08774*, 2023.

Abdul Fatir Ansari, Lorenzo Stella, Caner Turkmen, Xiyuan Zhang, Pedro Mercado, Huibin Shen, Oleksandr Shchur, Syama Sundar Rangapuram, Sebastian Pineda Arango, Shubham Kapoor, et al. Chronos: Learning the language of time series. *arXiv preprint arXiv:2403.07815*, 2024a.

Abdul Fatir Ansari, Caner Turkmen, Oleksandr Shchur, and Lorenzo Stella. Fast and accurate zero-shot forecasting with Chronos-Bolt and Autogluon, 2024b. URL https://aws.amazon.com/blogs/machine-learning/fast-and-accurate-zero-shot-forecasting-with-chronos-bolt-and-autogluon/.

Ane Blázquez-García, Angel Conde, Usue Mori, and Jose A Lozano. A review on outlier/anomaly detection in time series data. *ACM computing surveys (CSUR)*, 54(3):1–33, 2021.

Rishi Bommasani et al. On the opportunities and risks of foundation models. *arXiv preprint arXiv:2108.07258*, 2021.

Tom Brown, Benjamin Mann, Nick Ryder, Melanie Subbiah, Jared D Kaplan, Prafulla Dhariwal, Arvind Neelakantan, Pranav Shyam, Girish Sastry, Amanda Askell, et al. Language models are few-shot learners. *Advances in neural information processing systems*, 33:1877–1901, 2020.

Cristian Challu, Kin G Olivares, Boris N Oreshkin, Federico Garza Ramirez, Max Mergenthaler Canseco, and Artur Dubrawski. Nhits: Neural hierarchical interpolation for time series forecasting. In *Proceedings of the AAAI conference on artificial intelligence*, volume 37, pp. 6989–6997, 2023.

Anil Damle, Silke Glas, Alex Townsend, and Annan Yu. How to reveal the rank of a matrix? *arXiv preprint arXiv:2405.04330*, 2024.

Abhimanyu Das, Weihao Kong, Rajat Sen, and Yichen Zhou. A decoder-only foundation model for time-series forecasting. In *Forty-first International Conference on Machine Learning*, 2024.

Soham De and Samuel L. Smith. Batch normalization biases residual blocks towards the identity function in deep networks. In *Neural Information Processing Systems Foundation*, 2020.

Emily L Denton, Wojciech Zaremba, Joan Bruna, Yann LeCun, and Rob Fergus. Exploiting linear structure within convolutional networks for efficient evaluation. *Advances in neural information processing systems*, 27, 2014.

Alexey Dosovitskiy, Lucas Beyer, Alexander Kolesnikov, Dirk Weissenborn, Xiaohua Zhai, Thomas Unterthiner, Mostafa Dehghani, Matthias Minderer, Georg Heigold, Sylvain Gelly, et al. An image is worth 16x16 words: Transformers for image recognition at scale. *arXiv preprint arXiv:2010.11929*, 2020.

P. Drineas and M. W. Mahoney. RandNLA: Randomized numerical linear algebra. *Communications of the ACM*, 59:80–90, 2016.

Shibo Feng, Peilin Zhao, Liu Liu, Pengcheng Wu, and Zhiqi Shen. Hdt: Hierarchical discrete transformer for multivariate time series forecasting. *arXiv preprint arXiv:2502.08302*, 2025.

Everette S Gardner Jr. Exponential smoothing: The state of the art. *Journal of forecasting*, 4 (1):1–28, 1985.

Leon Götz, Marcel Kollovieh, Stephan Günnemann, and Leo Schwinn. Byte pair encoding for efficient time series forecasting. *arXiv preprint arXiv:2505.14411*, 2025.

Albert Gu and Tri Dao. Mamba: Linear-time sequence modeling with selective state spaces. *arXiv preprint arXiv:2312.00752*, 2023.

Albert Gu, Karan Goel, and Christopher Ré. Efficiently modeling long sequences with structured state spaces. *arXiv preprint arXiv:2111.00396*, 2021.

Albert Gu, Karan Goel, Ankit Gupta, and Christopher Ré. On the parameterization and initialization of diagonal state space models. *Advances in Neural Information Processing Systems*, 35:35971–35983, 2022.

Haokun Gui, Xiucheng Li, and Xinyang Chen. Vector quantization pretraining for eeg time series with random projection and phase alignment. In *International Conference on Machine Learning*, pp. 16731–16750. PMLR, 2024.

Tao Hong, Pierre Pinson, Shu Fan, Hamidreza Zareipour, Alberto Troccoli, and Rob J Hyndman. Probabilistic energy forecasting: Global energy forecasting competition 2014 and beyond, 2016.

Edward J Hu, Yelong Shen, Phillip Wallis, Zeyuan Allen-Zhu, Yuanzhi Li, Shean Wang, Lu Wang, Weizhu Chen, et al. Lora: Low-rank adaptation of large language models. *ICLR*, 1(2):3, 2022.

Rob J Hyndman and George Athanasopoulos. *Forecasting: principles and practice*. OTexts, 2018.

Ilse CF Ipsen and Arvind K Saibaba. Stable rank and intrinsic dimension of real and complex matrices. *arXiv preprint arXiv:2407.21594*, 2024.

Max Jaderberg, Andrea Vedaldi, and Andrew Zisserman. Speeding up convolutional neural networks with low rank expansions. *arXiv preprint arXiv:1405.3866*, 2014.

Yanrong Ji, Zhihan Zhou, Han Liu, and Ramana V Davuluri. Dnabert: pre-trained bidirectional encoder representations from transformers model for dna-language in genome. *Bioinformatics*, 37(15):2112–2120, 2021.

Jeffrey Lai, Anthony Bao, and William Gilpin. Panda: A pretrained forecast model for universal representation of chaotic dynamics. *arXiv preprint arXiv:2505.13755*, 2025.

Nguyen Quoc Khanh Le, Quang-Thai Ho, Trinh-Trung-Duong Nguyen, and Yu-Yen Ou. A transformer architecture based on bert and 2d convolutional neural network to identify dna enhancers from sequence information. *Briefings in bioinformatics*, 22(5):bbab005, 2021.

Vadim Lebedev, Yaroslav Ganin, Maksim Rakhuba, Ivan Oseledets, and Victor Lempitsky. Speeding-up convolutional neural networks using fine-tuned cp-decomposition. *arXiv preprint arXiv:1412.6553*, 2014.

Miguelangel Leon, Yuriy Perezhohin, Fernando Peres, Aleš Popovič, and Mauro Castelli. Comparing smiles and selfies tokenization for enhanced chemical language modeling. *Scientific Reports*, 14(1):25016, 2024.

Mike Lewis, Yinhan Liu, Naman Goyal, Marjan Ghazvininejad, Abdelrahman Mohamed, Omer Levy, Ves Stoyanov, and Luke Zettlemoyer. Bart: Denoising sequence-to-sequence pretraining for natural language generation, translation, and comprehension. *Proceedings of the 58th Annual Meeting of the Association for Computational Linguistics*, 2020.

Bryan Lim, Sercan Ö Arık, Nicolas Loeff, and Tomas Pfister. Temporal fusion transformers for interpretable multi-horizon time series forecasting. *International journal of forecasting*, 37 (4):1748–1764, 2021.

Ze Liu, Yutong Lin, Yue Cao, Han Hu, Yixuan Wei, Zheng Zhang, Stephen Lin, and Baining Guo. Swin transformer: Hierarchical vision transformer using shifted windows. In *Proceedings of the IEEE/CVF international conference on computer vision*, pp. 10012–10022, 2021.

Spyros Makridakis and Michele Hibon. Arma models and the box–jenkins methodology. *Journal of forecasting*, 16(3):147–163, 1997.

Charles H Martin and Michael W Mahoney. Implicit self-regularization in deep neural networks: Evidence from random matrix theory and implications for learning. *Journal of Machine Learning Research*, 22(165):1–73, 2021.

Luca Masserano, Abdul Fatir Ansari, Boran Han, Xiyuan Zhang, Christos Faloutsos, Michael W Mahoney, Andrew Gordon Wilson, Youngsuk Park, Syama Rangapuram, Danielle C Maddix, et al. Enhancing foundation models for time series forecasting via wavelet-based tokenization. In *International Conference on Machine Learning*. PMLR, 2025.

Łukasz Maziarka, Tomasz Danel, Sławomir Mucha, Krzysztof Rataj, Jacek Tabor, and Stanisław Jastrzebski. Molecule attention transformer. *arXiv preprint arXiv:2002.08264*, 2020.

Eric Nguyen, Michael Poli, Matthew G Durrant, Brian Kang, Dhruva Katrekar, David B Li, Liam J Bartie, Armin W Thomas, Samuel H King, Garyk Brixi, et al. Sequence modeling and design from molecular to genome scale with evo. *Science*, 386(6723):eado9336, 2024.

Yuqi Nie, Nam H Nguyen, Phanwadee Sinthong, and Jayant Kalagnanam. A time series is worth 64 words: Long-term forecasting with transformers. *arXiv preprint arXiv:2211.14730*, 2022.

Boris N Oreshkin, Dmitri Carpov, Nicolas Chapados, and Yoshua Bengio. N-beats: Neural basis expansion analysis for interpretable time series forecasting. *arXiv preprint arXiv:1905.10437*, 2019.

Alec Radford, Jong Wook Kim, Chris Hallacy, Aditya Ramesh, Gabriel Goh, Sandhini Agarwal, Girish Sastry, Amanda Askell, Pamela Mishkin, Jack Clark, et al. Learning transferable visual models from natural language supervision. In *International conference on machine learning*, pp. 8748–8763. PmLR, 2021.

David Salinas, Valentin Flunkert, Jan Gasthaus, and Tim Januschowski. Deepar: Probabilistic forecasting with autoregressive recurrent networks. *International journal of forecasting*, 36 (3):1181–1191, 2020.

Pratyusha Sharma, Jordan T Ash, and Dipendra Misra. The truth is in there: Improving reasoning in language models with layer-selective rank reduction. *arXiv preprint arXiv:2312.13558*, 2023.

Xiaoming Shi, Shiyu Wang, Yuqi Nie, Dianqi Li, Zhou Ye, Qingsong Wen, and Ming Jin. Time-moe: Billion-scale time series foundation models with mixture of experts. *International Conference on Learning Representations*, 2025.

Sabera Talukder, Yisong Yue, and Georgia Gkioxari. Totem: Tokenized time series embeddings for general time series analysis. *arXiv preprint arXiv:2402.16412*, 2024.

Alex Townsend and Lloyd N Trefethen. Continuous analogues of matrix factorizations. *Proceedings of the Royal Society A: Mathematical, Physical and Engineering Sciences*, 471(2173): 20140585, 2015.

Lloyd N Trefethen. *Approximation theory and approximation practice, extended edition*. SIAM, 2019.

Sinong Wang, Belinda Z Li, Madian Khabsa, Han Fang, and Hao Ma. Linformer: Self-attention with linear complexity. *arXiv preprint arXiv:2006.04768*, 2020.

Andrew Gordon Wilson. Deep learning is not so mysterious or different. *PMLR*, 2025.

Malcolm L Wolff, Shenghao Yang, Kari Torkkola, and Michael W Mahoney. Using pre-trained LLMs for multivariate time series forecasting. *arXiv preprint arXiv:2501.06386*, 2025.

Gerald Woo, Chenghao Liu, Akshat Kumar, Caiming Xiong, Silvio Savarese, and Doyen Sahoo. Unified training of universal time series forecasting transformers. 2024.

Yunyang Xiong, Zhanpeng Zeng, Rudrasis Chakraborty, Mingxing Tan, Glenn Fung, Yin Li, and Vikas Singh. Nyströmformer: A nyström-based algorithm for approximating self-attention. In *Proceedings of the AAAI conference on artificial intelligence*, volume 35, pp. 14138–14148, 2021.

Jinsung Yoon, William R Zame, and Mihaela Van Der Schaar. Estimating missing data in temporal data streams using multi-directional recurrent neural networks. *IEEE Transactions on Biomedical Engineering*, 66(5):1477–1490, 2018.

Annan Yu, Arnur Nigmetov, Dmitriy Morozov, Michael W Mahoney, and N Benjamin Erichson. Robustifying state-space models for long sequences via approximate diagonalization. *arXiv preprint arXiv:2310.01698*, 2023.

Annan Yu, Michael W Mahoney, and N Benjamin Erichson. Hope for a robust parameterization of long-memory state space models. *arXiv preprint arXiv:2405.13975*, 2024.

Michael Yuanjie Zhang, Jeffrey R Russell, and Ruey S Tsay. A nonlinear autoregressive conditional duration model with applications to financial transaction data. *Journal of Econometrics*, 104(1):179–207, 2001.

Xiyuan Zhang and Danielle Maddix Robinson. Mitra: Mixed synthetic priors for enhancing tabular foundation models, 2025. URL https://www.amazon.science/blog/mitra-mixed-synthetic-priors-for-enhancing-tabular-foundation-models.

Yuanzhao Zhang and William Gilpin. Zero-shot forecasting of chaotic systems. *International Conference on Learning Representations*, 2025.

A   Related Work

A.1   Time-series Modeling

Time series data are ubiquitous in many domains, including scientific (Abhishek et al., 2012; Zhang & Gilpin, 2025; Lai et al., 2025), industrial (Hong et al., 2016), and financial applications (Zhang et al., 2001), where they facilitate critical tasks, such as forecasting (Hyndman & Athanasopoulos, 2018), imputation (Yoon et al., 2018), and anomaly detection (Blázquez-García et al., 2021). Classical time-series forecasting (Hyndman & Athanasopoulos, 2018) has deep roots in traditional methods such as ARIMA (Makridakis & Hibon, 1997) and exponential smoothing (Gardner Jr, 1985). Many modern approaches involve deep learning; for example, sequence models such as DeepAR (Salinas et al., 2020) popularized probabilistic forecasting at scale, while Lim et al. (2021) combined the attention mechanism with interpretability for multi-horizon tasks. There are other neural forecasters without attention, such as N-BEATS (Oreshkin et al., 2019) and N-HiTS (Challu et al., 2023). An evolving modern alternative that targets long contexts efficiently is the recently developed state-space models (Gu et al., 2021) and Mamba (Gu & Dao, 2023). These neural-network-based methods are usually considered task-specific — that is, given a task, one trains a model to obtain a specific set of weights tailored to that task.

A.2   Time-series Foundation Models

Recent work pretrains general-purpose time series models across domains and tasks. Examples include TimesFM (Das et al., 2024), Chronos (Ansari et al., 2024a), Moirai (Woo et al., 2024), and Time MOE (Shi et al., 2025). These models differ in tokenization choices, training corpora, and zero-shot protocols, but they share the goal of one model that transfers across datasets and horizons.

A.3   Time-series Tokenization and Embedding

Designing the input representation is the key to leveraging the high flexibility and expressive power of large Transformers. Patching turns small motifs into tokens, as in Nie et al. (2022) and Das et al. (2024). Discrete tokenization via quantization has been explored by Ansari et al. (2024a) and Talukder et al. (2024), and other discrete designs include HDT (Feng et al., 2025) and vector-quantized methods (Gui et al., 2024). Another line of research is by using frequency-based tokenizers, such as WaveToken (Masserano et al., 2025). Lately, traditional language embedding strategies such as Byte-Pair Encoding are also considered (Götz et al., 2025).

A.4   Low-rank Structures in Deep Learning

Low-rank structure shows up in the deep learning community as both an inductive bias (Martin & Mahoney, 2021; Wilson, 2025; Yu et al., 2024) and a compression tool (Sharma et al., 2023; Gu et al., 2022; Yu et al., 2023). For attention, Linformer (Wang et al., 2020) and Nyströmformer (Xiong et al., 2021) explicitly approximate self-attention with low-rank projections. There is also a line of research that looks into parameter-efficient finetuning called LoRA (Hu et al., 2022), which learns low-rank updates to weight matrices. We note that LoRA is different from our low-rank model compression strategy because LoRA essentially learns a high-rank-plus-low-rank expression of the weight matrices, and does not facilitate storage or inference of a model. Earlier work reduced cost via matrix or tensor factorizations, especially in the CNN community (Denton et al., 2014; Jaderberg et al., 2014; Lebedev et al., 2014). These ideas suggest when low-rank operators suffice for sequence models, while our paper provides clean justifications for why low-rank operators suffice for a time-series foundation model.

B Proof of Theorem 1 and Corollary 2

Before we go into the proofs of Theorem 1 and Corollary 2, we present a figure to illustrate the differences between the quantization-based embedding and continuous embedding discussed in Section 2.
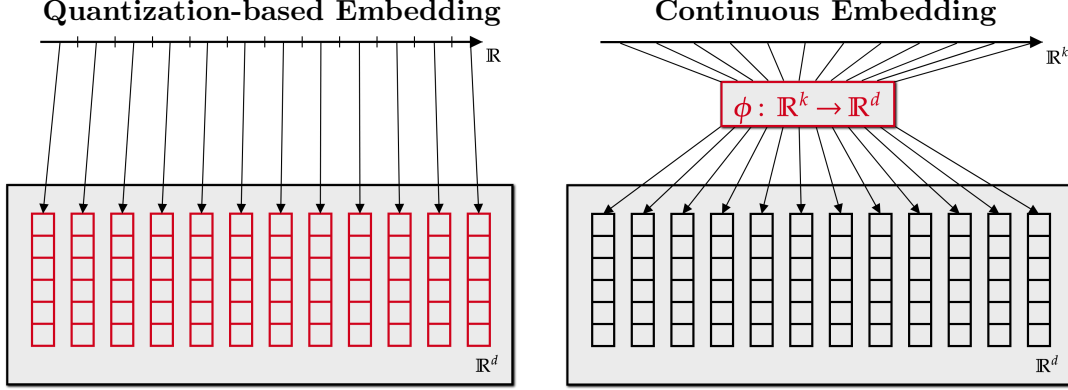

Figure 7: A comparison of the quantization-based embeddings and continuous embeddings. In a quantization-based one, we discretize the input domain into a number of regions and map each of them to a trainable vector. In a continuous embedding, we use a trainable function (usually an MLP) to map each element into the hidden space $\mathbb{R}^d$. The red parts in the figure highlight the trainable components.

The proof of Theorem 1 relies on classic polynomial approximation results. Intuitively, if a function ϕ is well-approximated by a low-degree polynomial, then the low-degree polynomial can be represented with a small basis, spanning a low-dimensional subspace. We now formalize this notion by providing the proof.

Proof of Theorem 1. Fix some $1 \leq j \leq d$. Let $P_{i,j}$ be the best degree-$(j-1)$ polynomial approximation of ϕ_i in the infinity norm, and let

$$\delta_j = \max_{1 \leq i \leq d} \|\phi_i - P_{i,j}\|_{L^\infty([-1,1])}.$$

Since $P_{i,j}$ is a polynomial of degree $\leq j - 1$, we can write it into

$$P_{i,j}(x) = \sum_{k=0}^{j-1} a_{i,k} \, T_k(x),$$

where T_k is the degree-k Chebyshev polynomial. Then, we can write $\boldsymbol{\Xi}$ into

$$\boldsymbol{\Xi} = \begin{bmatrix} — P_{1,j}(x) — \\ \vdots \\ — P_{d,j}(x) — \end{bmatrix} + \underbrace{\begin{bmatrix} — (\phi_1 - P_{1,j})(x) — \\ \vdots \\ — (\phi_d - P_{d,j})(x) — \end{bmatrix}}_{\mathbf{E}_j} = \underbrace{\begin{bmatrix} a_{1,0} & \cdots & a_{1,j-1} \\ \vdots & \ddots & \vdots \\ a_{d,0} & \cdots & a_{d,j-1} \end{bmatrix} \begin{bmatrix} — T_0(x) — \\ \vdots \\ — T_{j-1}(x) — \end{bmatrix}}_{\boldsymbol{\Xi}_j} + \mathbf{E}_j.$$

Since $\boldsymbol{\Xi}_j$ is a quasimatrix of rank at most j, by (Townsend & Trefethen, 2015, Thm. 4.2), we have that

$$s_{j+1} \leq \|\mathbf{E}_j\|_F = \sqrt{\sum_{i=1}^{d} \|\phi_i - P_{i,j}\|_{L^2([-1,1])}^2} \leq 2\sqrt{\sum_{i=1}^{d} \|\phi_i - P_{i,j}\|_{L^\infty([-1,1])}^2} \leq 2\sqrt{d}\,\delta_j. \quad (7)$$

Similarly, note that

$$
\boldsymbol{\Psi} = \begin{bmatrix} P_{1,j}(x_1) & \cdots & P_{1,j}(x_L) \\ \vdots & \ddots & \vdots \\ P_{d,j}(x_1) & \cdots & P_{d,j}(x_L) \end{bmatrix} + \underbrace{\begin{bmatrix} (\phi_1 - P_{1,j})(x_1) & \cdots & (\phi_1 - P_{1,j})(x_L) \\ \vdots & \ddots & \vdots \\ (\phi_d - P_{d,j})(x_1) & \cdots & (\phi_d - P_{d,j})(x_L) \end{bmatrix}}_{\mathbf{F}_j}
$$

$$
= \underbrace{\begin{bmatrix} a_{1,0} & \cdots & a_{1,j-1} \\ \vdots & \ddots & \vdots \\ a_{d,0} & \cdots & a_{d,j-1} \end{bmatrix} \begin{bmatrix} T_0(x_1) & \cdots & T_0(x_L) \\ \vdots & \ddots & \vdots \\ T_{j-1}(x_1) & \cdots & T_{j-1}(x_1) \end{bmatrix}}_{\boldsymbol{\Psi}_j} + \mathbf{F}_j.
$$

Since the rank of $\boldsymbol{\Psi}_j$ is at most j, by the Eckart–Young inequality, we have that

$$
\sigma_{j+1} \leq \|\mathbf{F}_j\|_2 \leq \|\mathbf{F}_j\|_F \leq \sqrt{dL}\delta_j. \tag{8}
$$

From (Trefethen, 2019, Thm. 7.2 & 8.2), we have that

$$
\delta_j \leq \frac{2V}{\pi\nu(j-1-\nu)^\nu} \qquad \text{and} \qquad \delta_j \leq \frac{2M\rho^{-j+1}}{\rho-1} \tag{9}
$$

when ϕ_i satisfies the condition in the first and the second statement of the theorem, respectively. Hence, the two statement are proved by combining eq. (7), (8), and (9). $\qquad\square$

The activation function swish_β used in Time MOE is analytic, and its domain of analyticity increases as $\beta \to 0^+$. Hence, we can use Theorem 1 to prove that Time MOE's embedding is low-rank.

Corollary 2. The embedding used in Time-MoE, defined by $\phi_i(x) = \text{swish}_\beta(w_i x) \cdot (v_i x) = (w_i v_i x^2)/(1 + e^{-\beta x})$, where we assume $|w_i v_i| \leq 1$ and $\beta > 0$, satisfies that

$$
\sigma_{j+1} = \mathcal{O}\left(\sqrt{dL}(\beta + \beta^{-1})(1 + \pi/(2\beta))^{-j+1}\right),
$$

where σ_{j+1} is defined in Theorem 1 for any $\boldsymbol{\Psi}$ and the constant in the $\mathcal{O}$-notation is universal.

Proof. The function $\phi_i(z)$ is a meromorphic function with poles at $\{z \mid \exp(-\beta z) = -1\} = \{(2k+1)\pi i/\beta \mid k \in \mathbb{Z}\}$. Set $\rho = 1 + \pi/(2\beta)$. Then, within the Bernstein ellipse E_ρ of radius ρ, we have that

$$
\text{Re}\left(e^{-\beta x}\right) > -c \Rightarrow |\phi_i(x)| \leq \frac{|x|^2}{1-c} = \mathcal{O}(1 + \beta^{-2}), \qquad x \in E_\rho,
$$

where $0 < c < 1$ is a universal constant and the constant in the $\mathcal{O}$-notation is also universal. The corollary follows from Theorem 1. $\qquad\square$

C Visualization of Tokenizers

In section 2, we consider a large corpus of inputs. Here, we perform two case studies to look into how each of the embeddings works. In particular, we select two time-series input data:

- A sinusoidal wave $\sin(t)$.

- A random Gaussian input, where each entry is i.i.d. $\mathcal{N}(0,1)$.

Let $\mathbf{X} \in \mathbb{R}^{d \times L}$ be the embedded input. For each pair of vectors $\mathbf{x}_i$ and $\mathbf{x}_j$ of $\mathbf{X}$, we compute the their correlation:

$$\theta_{i,j} = \arccos \left(\frac{|\mathbf{x}_i^\top \mathbf{x}_j|}{\|\mathbf{x}_i\|_2 \|\mathbf{x}_j\|_2} \right).$$

These correlation matrices are shown in Figure 8. There are two interesting observations to make: first, for WaveToken, the correlation matrix given a sinusoidal input has clearly four blocks — corresponding to the low-frequency wavelets and high-frequency ones. For Time MOE, the angles are so much darker because we apply a continuous embedding on a one-dimensional input space, leading to an ultimately low-rank structure.
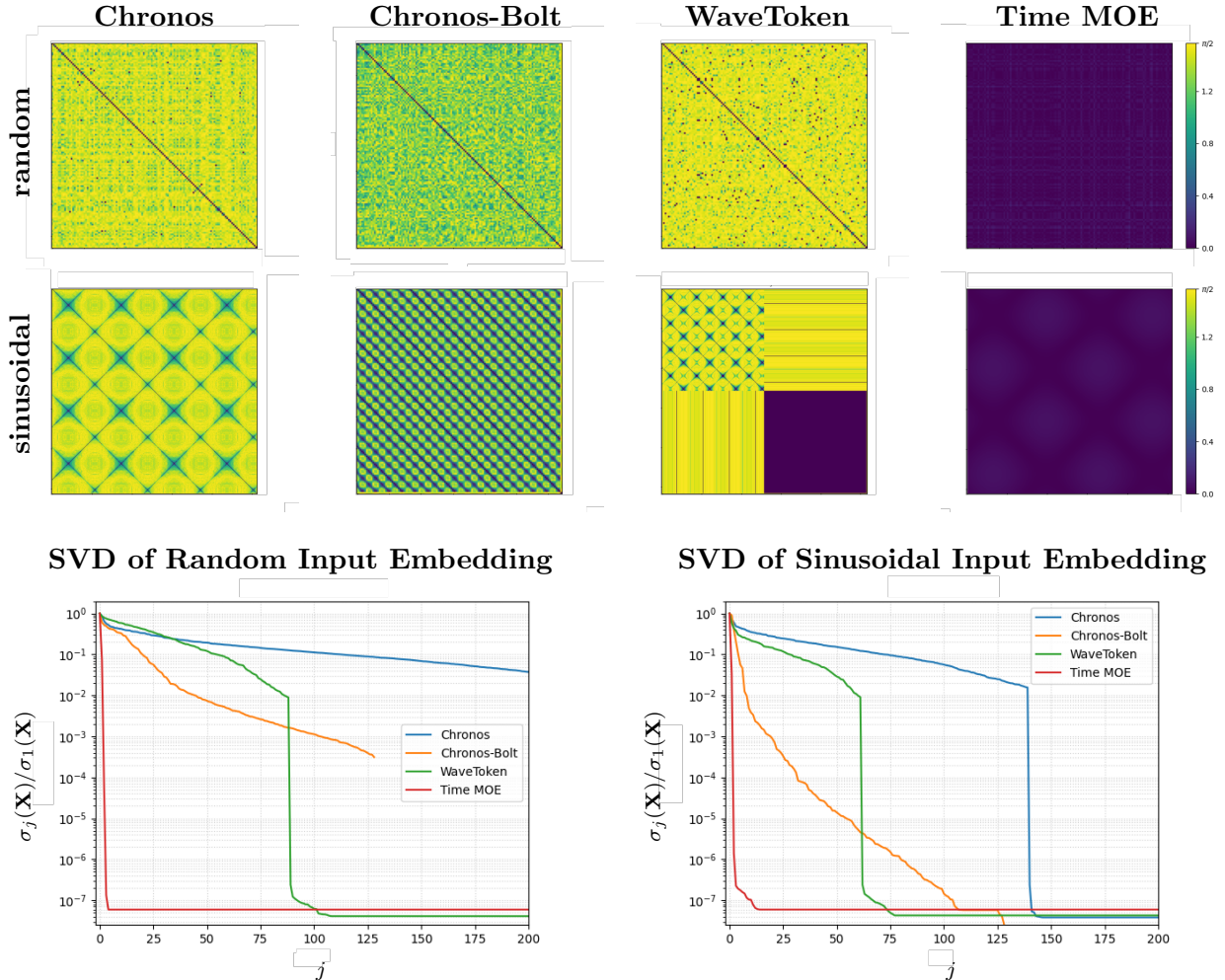

Figure 8: The heat maps show the correlation matrix of the embedded input with a random context or a sinusoidal one, using four different embedding strategies. The two line plots show the relative singular values of the embedded matrix $\mathbf{X}$.

We also observe that the numerical rank of the embedded input $\mathbf{X}$ is generally higher when the context is random than sinusoidal. This is not surprising either, because the temporal relationship within a random context is much more complex than that in a sinusoidal one.

D Proof of Theorem 2

The intuition in Theorem 2 is that if the MLP does not have a nonlinear activation function, then the linear MLP clearly maps a low-rank matrix to a low-rank matrix. While a nonlinear activation function complicates things, a contractive function does not increase the Frobenius norm of a matrix, which is equivalent to the ℓ^2-norm of all singular values.

Proof of Theorem 2. Since $\mathbf{X}$ is a rank-k matrix, the rank of $\mathbf{W}_1\mathbf{X}$ is at most k. Hence, the Frobenius norm of the matrix satisfies that

$$\|\mathbf{W}_1\mathbf{X}\|_F^2 = \sum_{j=1}^{k} \sigma_j(\mathbf{W}_1\mathbf{X})^2 \leq k\,\sigma_1(\mathbf{W}_1\mathbf{X})^2.$$

Given that $|\omega(x)| \leq |x|$ for every $x \in \mathbb{R}$, we have

$$k\,\sigma_1(\mathbf{W}_1\mathbf{X})^2 \geq \|\mathbf{W}_1\mathbf{X}\|_F^2 \geq \|\omega(\mathbf{W}_1\mathbf{X})\|_F^2 = \sum_{j=1}^{\min(d_f,L)} \sigma_j(\omega(\mathbf{W}_1\mathbf{X}))^2.$$

Using the singular value inequalities, we have that

$$\sum_{j=1}^{\min(d_f,L)} \sigma_j(\mathbf{W}_2\,\omega(\mathbf{W}_1\mathbf{X}))^2 \leq \sigma_1(\mathbf{W}_2)^2 \sum_{j=1}^{\min(d_f,L)} \sigma_j(\omega(\mathbf{W}_1\mathbf{X}))^2$$
$$\leq k\,\sigma_1(\mathbf{W}_2)^2\,\sigma_1(\mathbf{W}_1\mathbf{X})^2 = k\|\mathbf{W}_2\|_2^2\|\mathbf{W}_1\mathbf{X}\|_2^2.$$

This is, we can control the number of large singular values of $\mathbf{W}_2\,\omega(\mathbf{W}_1\mathbf{X})$ by

$$|\{j \mid \sigma_j(\mathbf{W}_2\,\omega(\mathbf{W}_1\mathbf{X})) > \varepsilon\|\mathbf{W}_2\|_2\|\mathbf{W}_1\mathbf{X}\|_2\}| \leq \varepsilon^{-2}k.$$

Moreover, the rank of the matrix $\mathbf{W}_3\mathbf{X}$ is at most k. Using the singular value inequality that

$$\sigma_{i+j-1}(\mathbf{A} + \mathbf{B}) \leq \sigma_i(\mathbf{A}) + \sigma_j(\mathbf{B}), \qquad \mathbf{A}, \mathbf{B} \in \mathbb{R}^{d \times L}, \quad i + j - 1 \leq \min(d, L),$$

we have

$$\sigma_{k+j}(\boldsymbol{\phi}(\mathbf{X})) \leq \sigma_{k+1}(\mathbf{W}_3\mathbf{X}) + \sigma_j(\mathbf{W}_2\,\omega(\mathbf{W}_1\mathbf{X})) = \sigma_j(\mathbf{W}_2\,\omega(\mathbf{W}_1\mathbf{X})), \quad j \leq \min(d, L) - k.$$

This gives us

$$|\{j \mid \sigma_j(\boldsymbol{\phi}(\mathbf{X})) > \varepsilon\|\mathbf{W}_2\|_2\|\mathbf{W}_1\mathbf{X}\|_2\}| \leq |\{j \mid \sigma_j(\mathbf{W}_2\,\omega(\mathbf{W}_1\mathbf{X})) > \varepsilon\|\mathbf{W}_2\|_2\|\mathbf{W}_1\mathbf{X}\|_2\}| + k$$
$$\leq (1 + \varepsilon^{-2})k,$$

which proves the result. $\qquad\square$

E   Proof of Theorem 3

To prove the upper bound in Theorem 3, we will prove a stronger result concerning not only a single-head attention but also a multi-head one.

Theorem 5. Let $C > 0$ be a constant. Let $\mathbf{\Xi} = \begin{bmatrix} \mathbf{x}_1 & \cdots & \mathbf{x}_N \end{bmatrix} \in \mathbb{R}^{d \times N}$ be an embedding matrix, where d is the hidden dimension, N is the vocabulary size, $\mathbf{x}_j \in \mathbb{R}^d$, and $\|\mathbf{x}_j\|_2 \le C$ for all $1 \le j \le N$. Let $\mathbf{W}_Q, \mathbf{W}_K, \mathbf{W}_V \in \mathbb{R}^{d \times d}$ be multi-head attention matrices with h heads, such that $\|(\mathbf{W}_Q^{(i)})^\top \mathbf{W}_K^{(i)}\|_2 \le C\sqrt{d_h}$, and $\|\mathbf{W}_V^{(i)}\|_2 \le C\sqrt{d_h}$ for every $1 \le i \le h$. For any $\tilde{d} < d$ such that $\sigma_{\tilde{d}+1} := \sigma_{\tilde{d}+1}(\mathbf{\Xi}) \le 1$, there exists a stable low-rank approximation $\tilde{\mathbf{W}}_Q, \tilde{\mathbf{W}}_K, \tilde{\mathbf{W}}_V \in \mathbb{R}^{d \times d}$ with $\mathrm{rank}(\tilde{\mathbf{W}}_Q) = \mathrm{rank}(\tilde{\mathbf{W}}_K) = \mathrm{rank}(\tilde{\mathbf{W}}_V) = \tilde{d}$, $\|\tilde{\mathbf{W}}_Q^\top \tilde{\mathbf{W}}_K\|_2 \le \|\mathbf{W}_Q^\top \mathbf{W}_K\|_2$, and $\|\tilde{\mathbf{W}}_V\|_2 \le \|\mathbf{W}_V\|_2$, such that given any input matrix $\mathbf{U} \in \mathbb{R}^{d \times L}$ for any $L \ge 1$, where each column of $\mathbf{U}$ is a column of $\mathbf{\Xi}$, we have that the low-rank attention matrices uniformly approximate the original one:

$$\left\| \text{MH-Attention}(\mathbf{U}; \mathbf{W}_Q, \mathbf{W}_K, \mathbf{W}_V, h) - \text{MH-Attention}(\mathbf{U}; \tilde{\mathbf{W}}_Q, \tilde{\mathbf{W}}_K, \tilde{\mathbf{W}}_V) \right\|_F \le \mathcal{O}\left(\sqrt{d}\, \sigma_{\tilde{d}+1} \right), \tag{10}$$

where the constant in the $\mathcal{O}$-notation only depends on C.

Proof. Fix a $\tilde{d} < d$. For the sake of simplicity, we assume, without loss of generality, that $C = 1$. Let

$$\mathbf{\Xi} = \mathbf{U}_{\tilde{d}} \mathbf{S}_{\tilde{d}} \mathbf{V}_{\tilde{d}}^\top, \qquad \mathbf{U}_{\tilde{d}} \in \mathbb{R}^{d \times \tilde{d}}, \quad \mathbf{S}_{\tilde{d}} \in \mathbb{R}^{\tilde{d} \times \tilde{d}}, \quad \mathbf{V}_{\tilde{d}} \in \mathbb{R}^{N \times \tilde{d}}$$

be the truncated SVD of $\mathbf{\Xi}$. Let $\mathbf{Q}_{\tilde{d}} = \mathbf{S}_{\tilde{d}} \mathbf{V}_{\tilde{d}}^\top \in \mathbb{R}^{\tilde{d} \times N}$. Therefore, we have

$$\|\mathbf{\Xi} - \mathbf{U}_{\tilde{d}} \mathbf{Q}_{\tilde{d}}\|_2 \le \sigma_{\tilde{d}+1}(\mathbf{\Xi}).$$

Define $\tilde{\mathbf{W}}_Q, \tilde{\mathbf{W}}_K$, and $\tilde{\mathbf{W}}_V$ by

$$\tilde{\mathbf{W}}_Q = \mathbf{W}_Q \mathbf{U}_{\tilde{d}} \mathbf{U}_{\tilde{d}}^\top \in \mathbb{R}^{d \times d}, \qquad \tilde{\mathbf{W}}_K = \mathbf{W}_K \mathbf{U}_{\tilde{d}} \mathbf{U}_{\tilde{d}}^\top \in \mathbb{R}^{d \times d}, \qquad \tilde{\mathbf{W}}_V = \mathbf{W}_V \mathbf{U}_{\tilde{d}} \mathbf{U}_{\tilde{d}}^\top \in \mathbb{R}^{d \times d}.$$

Since $\mathbf{U}_{\tilde{d}}$ has orthonormal columns, we have that $\|\mathbf{U}_{\tilde{d}}\|_2 = \|\mathbf{U}_{\tilde{d}}^\top\|_2 = 1$. By the sub-multiplicity of the spectral norm, we have that

$$\|\tilde{\mathbf{W}}_Q^\top \tilde{\mathbf{W}}_K\|_2 \le \|\mathbf{W}_Q^\top \mathbf{W}_K\|_2, \qquad \|\tilde{\mathbf{W}}_V\|_2 \le \|\mathbf{W}_V\|_2,$$

which proves the stability of the low-rank representation. Let $\mathbf{Q}_U \in \mathbb{R}^{\tilde{d} \times L}$ be the matrix defined by the condition that the ith column of $\mathbf{Q}_U$ is the jth column of $\mathbf{Q}_{\tilde{d}}$ if and only if the ith column of $\mathbf{U}$ is the jth column of $\mathbf{\Xi}$, and let

$$\mathbf{\Delta}_U = \mathbf{U}_{\tilde{d}} \mathbf{Q}_U - \mathbf{U}.$$

Since every column of $\mathbf{\Delta}_U$ is a column of $\mathbf{\Xi} - \mathbf{U}_{\tilde{d}} \mathbf{Q}_{\tilde{d}}$, its norm is no greater than $\sigma_{\tilde{d}+1}(\mathbf{\Xi})$, i.e.,

$$\begin{aligned} \|\mathbf{\Delta}_U(:,j)\|_2 &\le \sigma_{\tilde{d}+1}(\mathbf{\Xi}), \qquad 1 \le j \le L, \\ \|\mathbf{\Delta}_U\|_2 &\le \|\mathbf{\Delta}_U\|_F \le \sqrt{L} \sigma_{\tilde{d}+1}(\mathbf{\Xi}). \end{aligned} \tag{11}$$

Next, we have

$$\begin{aligned} \|\mathbf{\Delta}_V^{(i)}\|_2 &\le \|\mathbf{\Delta}_U^{(i)}\|_2 \le \sqrt{d_h L}\, \sigma_{\tilde{d}+1}(\mathbf{\Xi}), \\ \mathbf{\Delta}_V^{(i)} &:= \mathbf{W}_V^{(i)} \mathbf{U} - \tilde{\mathbf{W}}_V^{(i)} \mathbf{U} = \mathbf{W}_V^{(i)} \mathbf{U} - \mathbf{W}_V^{(i)} \mathbf{U}_{\tilde{d}} \mathbf{U}_{\tilde{d}}^\top \mathbf{U} \\ &= \mathbf{W}_V^{(i)} \mathbf{U} - \mathbf{W}_V^{(i)} \mathbf{U}_{\tilde{d}} \mathbf{U}_{\tilde{d}}^\top \mathbf{U}_{\tilde{d}} \mathbf{Q}_U \\ &= \mathbf{W}_V^{(i)} \mathbf{U} - \mathbf{W}_V^{(i)} \mathbf{U}_{\tilde{d}} \mathbf{Q}_U = -\mathbf{W}_V^{(i)} \mathbf{\Delta}_U, \end{aligned}$$

where the first inequality comes from the sub-multiplicity of the spectral norm. Moreover, every column of $\mathbf{\Delta}_V^{(i)}$ is a column of $-\mathbf{W}_V^{(i)}\mathbf{\Delta}_U$ and must satisfy that

$$\|\mathbf{\Delta}_V^{(i)}(:,j)\|_2 \le \sqrt{d_h}\,\sigma_{\tilde{d}+1}(\mathbf{\Xi}), \qquad 1 \le j \le L. \tag{12}$$

Similarly, we have that

$$\begin{aligned}
\|\mathbf{\Delta}_Q^{(i)}\|_2 &\le \sqrt{d_h}\,L(2\sigma_{\tilde{d}+1}(\mathbf{\Xi}) + \sigma_{\tilde{d}+1}(\mathbf{\Xi})^2), \\
\mathbf{\Delta}_Q^{(i)} &:= \mathbf{U}^\top(\mathbf{W}_Q^{(i)})^\top\mathbf{W}_K^{(i)}\mathbf{U} - \mathbf{U}^\top(\tilde{\mathbf{W}}_Q^{(i)})^\top\tilde{\mathbf{W}}_K^{(i)}\mathbf{U} \\
&= \mathbf{U}^\top(\mathbf{W}_Q^{(i)})^\top\mathbf{W}_K^{(i)}\mathbf{U} - \mathbf{U}^\top\mathbf{U}_{\tilde{d}}\mathbf{U}_{\tilde{d}}^\top(\mathbf{W}_Q^{(i)})^\top\mathbf{W}_K^{(i)}\mathbf{U}_{\tilde{d}}\mathbf{U}_{\tilde{d}}^\top\mathbf{U} \\
&= \mathbf{U}^\top(\mathbf{W}_Q^{(i)})^\top\mathbf{W}_K^{(i)}\mathbf{U} - \mathbf{Q}_X^\top\mathbf{U}_{\tilde{d}}^\top(\mathbf{W}_Q^{(i)})^\top\mathbf{W}_K^{(i)}\mathbf{U}_{\tilde{d}}\mathbf{Q}_U \\
&= -\mathbf{\Delta}_U^\top(\mathbf{W}_Q^{(i)})^\top\mathbf{W}_K^{(i)}\mathbf{U} - \mathbf{U}^\top(\mathbf{W}_Q^{(i)})^\top\mathbf{W}_K^{(i)}\mathbf{\Delta}_U - \mathbf{\Delta}_U^\top(\mathbf{W}_Q^{(i)})^\top\mathbf{W}_K^{(i)}\mathbf{\Delta}_U,
\end{aligned}$$

where the inequality is obtained by recalling that $\|\mathbf{U}\|_2 \le \sqrt{L}$ and $\|\mathbf{\Delta}_U\|_2 \le \sqrt{L}\,\sigma_{\tilde{d}+1}(\mathbf{\Xi})$. Moreover, since we have $\|\mathbf{U}(:,j)\|_2 \le 1$ and $\|\mathbf{\Delta}_U(:,j)\|_2 \le \sigma_{\tilde{d}+1}(\mathbf{\Xi})$ for all $1 \le j \le N$, every entry of $\mathbf{\Delta}_Q^{(i)}$ satisfies that

$$\|\mathbf{\Delta}_Q^{(i)}(t,j)\|_2 \le \sqrt{d_h}(2\sigma_{\tilde{d}+1}(\mathbf{\Xi}) + \sigma_{\tilde{d}+1}(\mathbf{\Xi})^2), \qquad 1 \le t \le L, \quad 1 \le j \le L. \tag{13}$$

For each fixed $1 \le i \le h$, define the notations

$$\mathbf{G}^{(i)} = \frac{\mathbf{U}^\top(\mathbf{W}_Q^{(i)})^\top\mathbf{W}_K^{(i)}\mathbf{U}}{\sqrt{d_h}}, \qquad \tilde{\mathbf{G}}^{(i)} = \frac{\mathbf{U}^\top(\tilde{\mathbf{W}}_Q^{(i)})^\top\tilde{\mathbf{W}}_K\mathbf{U}}{\sqrt{d_h}},$$

$$\boldsymbol{g}_j^{(i)} = \mathbf{G}(:,j), \qquad\qquad \tilde{\boldsymbol{g}}_j^{(i)} = \tilde{\mathbf{G}}(:,j).$$

For simplicity, we drop the superscripts (i) on $\mathbf{G}$, $\tilde{\mathbf{G}}$, $\boldsymbol{g}$, and $\tilde{\boldsymbol{g}}$. Since we assumed $\|\mathbf{u}_j\|_2 \le 1$ for all $1 \le j \le N$ and $\|(\mathbf{W}_Q^{(i)})^\top\mathbf{W}_K^{(i)}\|_2 \le \sqrt{d_h}$, we have that

$$\|\boldsymbol{g}_j\|_{\max} \le 1, \qquad \|\tilde{\boldsymbol{g}}_j\|_{\max} \le 1, \qquad 1 \le j \le L.$$

Denote by g_j^t and $\tilde{g}_j^t$ the tth entry of $\boldsymbol{g}_j$ and $\tilde{\boldsymbol{g}}_j$, respectively. For every fixed $1 \le j \le L$ and $1 \le t \le L$, we have

$$\begin{aligned}
|\underbrace{\mathrm{softmax}(\boldsymbol{g}_j)^t - \mathrm{softmax}(\tilde{\boldsymbol{g}}_j)^t}_{d_j^t}| &= \left| \frac{\exp(g_j^t)}{\sum_{k=1}^L \exp(g_j^k)} - \frac{\exp(\tilde{g}_j^t)}{\sum_{k=1}^L \exp(\tilde{g}_j^k)} \right| \\
&= \frac{\left| \sum_{k=1}^L \left(\exp(g_j^t)\exp(\tilde{g}_j^k) - \exp(\tilde{g}_j^t)\exp(g_j^k) \right) \right|}{\left| \left(\sum_{k=1}^L \exp(g_j^k) \right) \left(\sum_{k=1}^L \exp(\tilde{g}_j^k) \right) \right|} \le \frac{L\max_k \left| \exp(g_j^t)\exp(\tilde{g}_j^k) - \exp(\tilde{g}_j^t)\exp(g_j^k) \right|}{L^2 \exp(-2)} \\
&= \frac{L\max_k \left| \exp(g_j^t)(\exp(g_j^k) + (\exp(\tilde{g}_j^k) - \exp(g_j^k))) - (\exp(g_j^t) + (\exp(\tilde{g}_j^t) - \exp(g_j^t)))\exp(g_j^k) \right|}{L^2 \exp(-2)} \\
&\le \frac{\max_k \left(\exp(1) \left(|\exp(g_j^k) - \exp(\tilde{g}_j^k)| + |\exp(g_j^t) - \exp(\tilde{g}_j^t)| \right) + |\exp(g_j^k) - \exp(\tilde{g}_j^k)||\exp(g_j^t) - \exp(\tilde{g}_j^t)| \right)}{L\exp(-2)} \\
&\le \underbrace{\frac{2\exp(1)(2\sigma_{\tilde{d}+1}(\mathbf{\Xi}) + \sigma_{\tilde{d}+1}(\mathbf{\Xi})^2) + (2\sigma_{\tilde{d}+1}(\mathbf{\Xi}) + \sigma_{\tilde{d}+1}(\mathbf{\Xi})^2)^2}{L\exp(-2)}}_{D_Q},
\end{aligned}$$

$$\tag{14}$$

where the last inequality follows from eq. (13). Hence, for each fixed $1 \leq j \leq L$ and $1 \leq i \leq h$, we have that

$$\left\| \mathbf{W}_V^{(i)} \mathbf{U} \, \mathrm{softmax}(\boldsymbol{g}_j^{(i)}) - \tilde{\mathbf{W}}_V^{(i)} \mathbf{U} \, \mathrm{softmax}(\tilde{\boldsymbol{g}}_j^{(i)}) \right\|_2$$

$$= \left\| \sum_{i=1}^{L} \left(\mathbf{W}_V^{(i)} \mathbf{U}(:,i) \, \mathrm{softmax}(g_j^t) - \tilde{\mathbf{W}}_V^{(i)} \mathbf{U}(:,i) \, \mathrm{softmax}(\tilde{g}_j^t) \right) \right\|_2$$

$$\leq \sqrt{L} \max_{1 \leq t \leq L} \left\| \left(\mathbf{W}_V^{(i)} \mathbf{U}(:,t) \, \mathrm{softmax}(g_j^t) - (\mathbf{W}_V^{(i)} \mathbf{U}(:,t) - \boldsymbol{\Delta}_V^{(i)}(:,t)) \, (\mathrm{softmax}(g_j^t) - d_j^t) \right) \right\|_2$$

$$\leq \sqrt{L} \max_{1 \leq t \leq L} \left(\|\boldsymbol{\Delta}_V^{(i)}(:,t)\|_2 |\mathrm{softmax}(\tilde{g}_j^t)| + \|\mathbf{W}_V^{(i)} \mathbf{U}(:,t)\|_2 \, D_Q \right)$$

$$\leq \sqrt{L} \left(\sqrt{d_h} \, \sigma_{\tilde{d}+1} \Theta(1/L) + \sqrt{d_h} \, \mathcal{O}\left(\left(\sigma_{\tilde{d}+1} + \sigma_{\tilde{d}+1}^2 \right) / L \right) \right) = \mathcal{O}\left(\sqrt{d_h} \, \sigma_{\tilde{d}+1} / \sqrt{L} \right),$$

where the last inequality follows from eq. (12) and (14). Since we have $\mathbf{W}_V^{(i)} \mathbf{U} \, \mathrm{softmax}(\boldsymbol{g}_j^{(i)}) - \tilde{\mathbf{W}}_V^{(i)} \mathbf{U} \, \mathrm{softmax}(\tilde{\boldsymbol{g}}_j^{(i)})$ is the jth column of

$$\mathrm{Attention}(\mathbf{U}; \mathbf{W}_Q^{(i)}, \mathbf{W}_K^{(i)}, \mathbf{W}_V^{(i)}) - \mathrm{Attention}(\mathbf{U}; \tilde{\mathbf{W}}_Q^{(i)}, \tilde{\mathbf{W}}_K^{(i)}, \tilde{\mathbf{W}}_V^{(i)}),$$

we have that

$$\|\mathrm{MH\text{-}Attention}(\mathbf{U}; \mathbf{W}_Q, \mathbf{W}_K, \mathbf{W}_V, h) - \mathrm{Attention}(\mathbf{U}; \tilde{\mathbf{W}}_Q, \tilde{\mathbf{W}}_K, \tilde{\mathbf{W}}_V, h)\|_F$$

$$= \sqrt{\sum_{i=1}^{h} \|\mathrm{Attention}(\mathbf{U}; \mathbf{W}_Q^{(i)}, \mathbf{W}_K^{(i)}, \mathbf{W}_V^{(i)}) - \mathrm{Attention}(\mathbf{U}; \tilde{\mathbf{W}}_Q^{(i)}, \tilde{\mathbf{W}}_K^{(i)}, \tilde{\mathbf{W}}_V^{(i)})\|_F^2}$$

$$\leq \sqrt{\sum_{i=1}^{h} \sum_{j=1}^{L} \left\| \mathbf{W}_V^{(i)} \mathbf{U} \, \mathrm{softmax}(\boldsymbol{g}_j^{(i)}) - \tilde{\mathbf{W}}_V^{(i)} \mathbf{U} \, \mathrm{softmax}(\tilde{\boldsymbol{g}}_j^{(i)}) \right\|_2^2}$$

$$= \sqrt{hL} \mathcal{O}\left(\sqrt{d_h} \, \sigma_{\tilde{d}+1} / \sqrt{L} \right) = \mathcal{O}\left(\sqrt{d} \, \sigma_{\tilde{d}+1} \right).$$

The proof is complete. $\qquad\qquad\square$

Theorem 5 immediately proves the upper bound in Theorem 3. The lower bound needs a separate argument.

Proof of Theorem 3. The upper bound follows immediately from Theorem 5 by setting $h = 1$. To prove the lower bound, let $\mathbf{U}' \in \mathbb{R}^{d \times \tilde{d}}$ and $\mathbf{U} \in \mathbb{R}^{d \times L}$ be such that

$$\mathbf{U} = \left[\begin{array}{c|c} \mathbf{U}' & \mathbf{0} \end{array} \right], \qquad \mathbf{U}' = \mathrm{diag}(\sigma_1, \ldots, \sigma_d) \in \mathbb{R}^{d \times d}, \quad \mathbf{0} \in \mathbb{R}^{d \times (L-d)}.$$

Clearly, the singular values of $\mathbf{U}$ are $\sigma_1, \ldots, \sigma_d$. Define $\mathbf{W}_Q$ and $\mathbf{W}_K$ such that

$$\mathbf{W}_Q^\top \mathbf{W}_K = \log(4d) \sigma_d^{-2} \sqrt{d} \, \mathbf{I}_d.$$

Then, we have

$$\mathbf{T} := \frac{\mathbf{U}^\top \mathbf{W}_Q^\top \mathbf{W}_K \mathbf{U}}{\sqrt{d}} = \log(4d) \sigma_d^{-2} \left[\begin{array}{c|c} \mathrm{diag}(\sigma_1^2, \ldots, \sigma_d^2) & \mathbf{0}_{d \times (L-d)} \\ \hline \mathbf{0}_{(L-d) \times d} & \mathbf{0}_{(L-d) \times (L-d)} \end{array} \right].$$

Let $\mathbf{G} = \mathrm{softmax}(\mathbf{T})$ and let $\boldsymbol{g}_j$ be the jth column of $\mathbf{G}$. Then, for every $1 \leq j \leq d$, we have

$$\boldsymbol{g}_j = [g_j^1, \ldots, g_j^L]^\top, \qquad g_j^i = \begin{cases} \dfrac{1}{(L-1) + \exp\left(\log(4d)\sigma_d^{-2}\sigma_j^2\right)} \leq \dfrac{1}{4d}, & i \neq j, \\[4mm] \dfrac{\exp\left(\log(4d)\sigma_d^{-2}\sigma_j^2\right)}{(L-1) + \exp\left(\log(4d)\sigma_d^{-2}\sigma_j^2\right)} \geq \dfrac{1}{2}, & i = j. \end{cases} \tag{15}$$

Write $\mathbf{G}$ into
$$\mathbf{G} = \left[\begin{array}{c|c} \mathbf{G}_{11} & \mathbf{G}_{12} \\ \hline \mathbf{G}_{21} & \mathbf{G}_{22} \end{array} \right],$$
where
$$\mathbf{G}_{11} = \mathbf{G}' \in \mathbb{R}^{d \times d}, \quad \mathbf{G}_{12} \in \mathbb{R}^{d \times (L-d)}, \quad \mathbf{G}_{21} \in \mathbb{R}^{(L-d) \times d}, \quad \mathbf{G}_{22} \in \mathbb{R}^{(L-d) \times (L-d)},$$
and write $\mathbf{G}_{11}$ into the sum of its diagonal part and off-diagonal part:
$$\mathbf{G}_{11} = \mathbf{G}_{\text{diag}} + \mathbf{G}_{\text{off-diag}},$$
where $\mathbf{G}_{\text{diag}}$ is a diagonal matrix and $\mathbf{G}_{\text{off-diag}}$ is a matrix with zero diagonal entries. Then, by eq. (15), we have
$$\sigma_d(\mathbf{G}_{\text{diag}}) = \min_{1 \leq j \leq d} g_j^j \geq \frac{1}{2}, \qquad \|\mathbf{G}_{\text{off-diag}}\|_2 \leq \|\mathbf{G}_{\text{off-diag}}\|_F \leq d \frac{1}{4d} = \frac{1}{4}.$$

Hence, by Weyl's inequality, we have
$$\sigma_d(\mathbf{G}_{11}) \geq \sigma_d(\mathbf{G}_{\text{diag}}) - \|\mathbf{G}_{\text{off-diag}}\|_2 \geq \frac{1}{4}. \tag{16}$$

Using the results above, we have
$$\mathbf{W}_V \mathbf{U} \, \text{softmax}\left(\frac{\mathbf{U}^\top \mathbf{W}_Q^\top \mathbf{W}_K \mathbf{U}}{\sqrt{d}} \right) - \tilde{\mathbf{W}}_V \mathbf{U} \, \text{softmax}\left(\frac{\mathbf{U}^\top \mathbf{W}_Q^\top \mathbf{W}_K \mathbf{U}}{\sqrt{d}} \right)$$
$$= (\mathbf{W}_V \mathbf{U} - \tilde{\mathbf{W}}_V \mathbf{U}) \mathbf{G} = \left[\begin{array}{c|c} \mathbf{W}_V \mathbf{U}' - \tilde{\mathbf{W}}_V \mathbf{U}' & \mathbf{0}_{d \times (L-d)} \end{array} \right] \left[\begin{array}{c|c} \mathbf{G}_{11} & \mathbf{G}_{12} \\ \hline \mathbf{G}_{21} & \mathbf{G}_{22} \end{array} \right]$$
$$= \left[\begin{array}{c|c} \left(\mathbf{W}_V \mathbf{U}' - \tilde{\mathbf{W}}_V \mathbf{U}' \right) \mathbf{G}_{11} & \left(\mathbf{W}_V \mathbf{U}' - \tilde{\mathbf{W}}_V \mathbf{U}' \right) \mathbf{G}_{12} \end{array} \right],$$
but $\tilde{\mathbf{W}}_V \mathbf{U}'$ is a rank-$\tilde{d}$ matrix so we must have
$$\|\mathbf{W}_V \mathbf{U}' - \tilde{\mathbf{W}}_V \mathbf{U}'\|_2 \geq \sigma_{\tilde{d}+1}(\mathbf{W}_V \mathbf{U}') = \sigma_{\tilde{d}+1}. \tag{17}$$

Hence, by the singular value inqualities, we have
$$\left\| \mathbf{W}_V \mathbf{U} \, \text{softmax}\left(\frac{\mathbf{U}^\top \mathbf{W}_Q^\top \mathbf{W}_K \mathbf{U}}{\sqrt{d}} \right) - \tilde{\mathbf{W}}_V \mathbf{U} \, \text{softmax}\left(\frac{\mathbf{U}^\top \mathbf{W}_Q^\top \mathbf{W}_K \mathbf{U}}{\sqrt{d}} \right) \right\|_2$$
$$\geq \left\| \left(\mathbf{W}_V \mathbf{U}' - \tilde{\mathbf{W}}_V \mathbf{U}' \right) \mathbf{G}_{11} \right\|_2 \geq \sigma_1 \left(\mathbf{W}_V \mathbf{U}' - \tilde{\mathbf{W}}_V \mathbf{U}' \right) \sigma_d(\mathbf{G}_{11}) \geq \frac{1}{4} \sigma_{\tilde{d}+1},$$

where the last inequality is obtained by combining eq. (16) and (17). The proof is complete. $\quad \square$

F   Numerical Experiments to Corroborate Our Theorem

In this appendix, we provide numerical experiments, simulated in MATLAB R2024b, that verify the theoretical statements we made in the main manuscript.

F.1   Two Numerical Experiments on Theorem 3

To verify Theorem 3, we fix the hidden dimension to be $d = 512$ and the vocabulary size $N = 4096$. We create a random embedded matrix $\mathbf{X} \in \mathbb{R}^{d \times N}$ with singular values $\mathbf{s} \in \mathbb{R}^d$ ranging from e^{-5} to e^0 and uniformly distributed on a logarithmic scale. This matrix is computed by randomly sampling an orthogonal matrix $\mathbf{U} \in \mathbb{R}^{d \times d}$ and a matrix $\mathbf{V} \in \mathbb{R}^{N \times d}$ with orthonormal columns, via QR-decomposing random matrices, and setting $\mathbf{X} = \mathbf{U} \operatorname{diag}(\mathbf{s}) \mathbf{V}^\top$.

Next, we randomly sample three attention matrices $\mathbf{W}_Q, \mathbf{W}_K, \mathbf{W}_V$, and for each reduced-order $\tilde{d} = 1, \ldots, d - 1$, we use the constructive formulas given in the proof of Theorem 3 to compute the reduced matrices $\tilde{\mathbf{W}}_Q, \tilde{\mathbf{W}}_K, \tilde{\mathbf{W}}_V$. We set the input to be the entire vocabulary matrix $\mathbf{X}$ and compute the output of the original attention layer, defined by $\mathbf{W}_Q, \mathbf{W}_K, \mathbf{W}_V$, as well as that of the reduced one, defined by $\tilde{\mathbf{W}}_Q, \tilde{\mathbf{W}}_K, \tilde{\mathbf{W}}_V$. We evaluate the Frobenius norm of the difference between the two outputs.
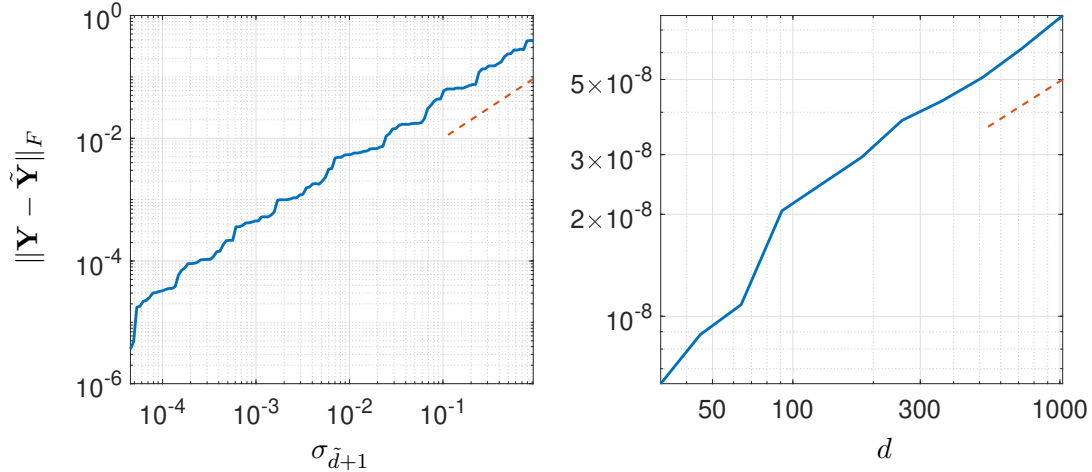

Figure 9: The left panel shows the relationship between the reduced-order $\tilde{d}$ and the approximation error of a randomly sampled attention layer applied to a randomly sampled input matrix $\mathbf{X}$ with controlled singular values $\sigma_1, \ldots, \sigma_d$. The reference line has a slope of 1 in the log-log plot. The right panel shows the relationship between the dimension of the hidden space d and the approximation error of a fixed-degree reduced-order model. For each hidden space d, we randomly resample the attention matrices and embedded matrix $\mathbf{X}$, holding its leading singular values unchanged. The reference line has a slope of $1/2$ in the log-log plot.

Figure 9 shows two controlled experiments by changing a different variable. On the left, we change the truncation degree $\tilde{d}$, which in turn controls the singular value $\sigma_{\tilde{d}+1}$. The reference line has a slope of 1, revealing a linear relationship between $\|\mathbf{Y} - \tilde{\mathbf{Y}}\|_F$ and $\sigma_{\tilde{d}+1}$, as indicated in Theorem 3. On the right, we change the size of the hidden space d, and the reference line has a slope of $1/2$, which verifies the $\sqrt{d}$ factor in the statement of Theorem 3.

F.2   A Numerical Experiment on Theorem 6

The essence of Theorem 6 is that a sparse multi-head sketching is more effective than a dense single-head sketching. We use an experiment to verify that. In our setting, we set $d = 2048$ and

$L = 4096$, and we randomly sample an input matrix $\mathbf{X} \in \mathbb{R}^{d \times L}$ with exponentially decaying singular values, as shown in the left panel of Figure 10. Our sampling method is the same as the one outlined in the previous experiment.
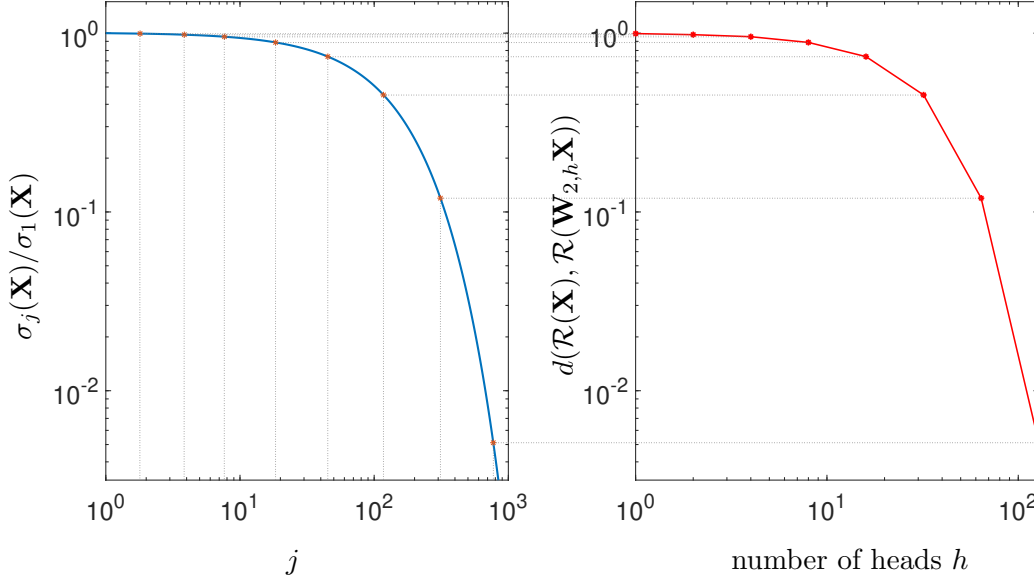

Figure 10: On the left, we show the singular values of the input matrices. On the right, we compute the "sketching error" defined in eq. (18), as we change the number of heads in a sparse sketching. We map the sketching errors back to the singular value plot to indicate the index j such that our sketching error achieves an error below σ_{j+1}.

We set our reduced rank to $\tilde{d} = 4$. If we just use a single head to sketch a rank-$\tilde{d}$ space from the row space of $\mathbf{X}$, then its accuracy is lower-bounded by $\sigma_{\tilde{d}+1}$, which is still a large number. To explore the potential of sparse head-dependent sketching, we increase the number of heads from $h = 1$ to 128 and keep it an integral divisor of d. For each h, we use the sparse sketching; that is, we assemble a random matrix

$$\mathbf{W}_{2,h} = \begin{bmatrix} \mathbf{W}_{2,h}^{(1),\top} & \cdots & \mathbf{W}_{2,h}^{(1),\top} \end{bmatrix}^\top, \qquad \mathbf{W}_{2,h}^{(i)} \in \mathbb{R}^{\tilde{d} \times d}.$$

The matrix $\mathbf{W}_{2,h}$ is sparse in the sense that it has exactly $d_h = d/h$ non-zero entries, whose positions are randomly chosen, and for each non-zero position, we sample its value i.i.d. from $\mathcal{N}(0,1)$. Note that given this sparse design, $\mathbf{W}_{2,h}$ has the same number of non-zero entries for any h.

Now, our question is: what is the different between the row space of $\mathbf{W}_{2,h}\mathbf{X}$ and that of $\mathbf{X}$? In other words, how good is the sketching using $\mathbf{W}_{2,h}$? To this end, we clearly have that $\mathcal{R}(\mathbf{W}_{2,h}\mathbf{X}) \subset \mathcal{R}(\mathbf{X})$, where we use the notation $\mathcal{R}$ for the row space of a matrix. Hence, the remaining question is how much in $\mathcal{R}(\mathbf{X})$ is not filled by $\mathcal{R}(\mathbf{W}_{2,h}\mathbf{X})$. This can be measured by projecting $\mathcal{R}(\mathbf{X})$ onto $\mathcal{R}(\mathbf{W}_{2,h}\mathbf{X})$ and measure the loss by the projection:

$$d(\mathcal{R}(\mathbf{X}), \mathcal{R}(\mathbf{W}_{2,h}\mathbf{X})) = \left\| \mathrm{orth}(\mathbf{X}^\top \mathbf{W}_{R,h}^\top) \, \mathrm{orth}(\mathbf{X}^\top \mathbf{W}_{R,h}^\top)^\top \mathbf{X}^\top - \mathbf{X}^\top \right\|_2. \tag{18}$$

We show this distance in the right panel of Figure 10, and we relate this to the singular values of $\mathbf{X}$. In that sense, since the vertical rules in the left panel are almost evenly spaced, it shows that the "effective rank" of $\mathcal{R}(\mathbf{W}_{2,h}\mathbf{X})$ grows proportionally with respect to h, indicating that the quality of a sparse multi-head sketching is comparable to the quality of a dense multi-head sketching.

F.3 A Numerical Experiment on Theorem 4

Our final numerical experiment considers the flow-of-ranks. Theorem 4 suggests that a larger number of heads also facilitates the flow-of-rank, and this is hard to validate empirically with pretrained Chronos models. In our targeted numerical experiment, we fix an input matrix $\mathbf{X}$ with predefined exponentially decaying singular values, which is, again, randomly sampled from the product of a random orthogonal matrix, a predefined diagonal matrix, and the transpose of a random matrix with orthonormal columns (see the previous two subsections). Then, we randomly select $\mathbf{W}_Q, \mathbf{W}_K, \mathbf{W}_V$ and compute the output of the attention mechanism defined by these three matrices together with a number of heads parameter h. Figure 11 gives us that the output matrix

$$\mathbf{Y} = \text{MH-Attention}(\mathbf{X}; \mathbf{W}_Q, \mathbf{W}_K, \mathbf{W}_V, h) + \mathbf{X}$$
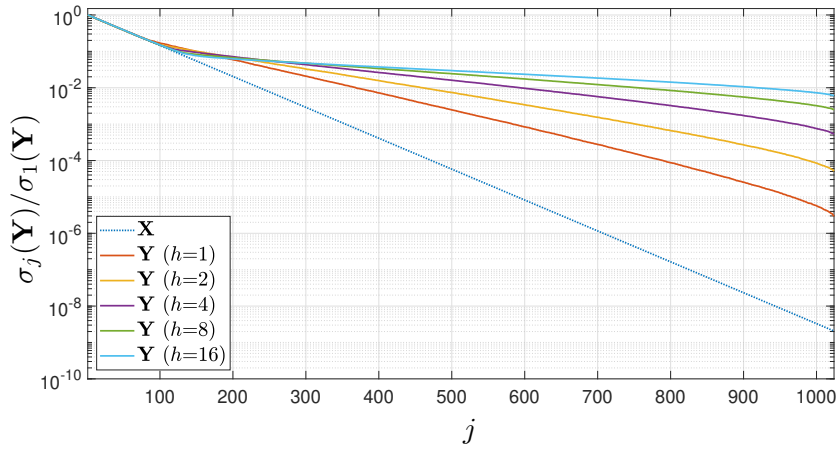
is higher-rank as h increases.

Figure 11: Relative singular values of the input matrix $\mathbf{X}$ and output matrices $\mathbf{Y} = \text{MH-Attention}(\mathbf{X}; \mathbf{W}_Q, \mathbf{W}_K, \mathbf{W}_V, h) + \mathbf{X}$ as we change the number of heads h. We see that the numerical rank of $\mathbf{Y}$ increases with h.

G   Watching the Weights of Large Models

The central claims made in this paper are heavily based on the low-rank structures of weight matrices in large-scale time series foundation models. In this section, we provide more empirical analysis of the singular values of these matrices.

G.1   Comparing the Weights of TSFMs and LLMs

For the first set of comparisons, we consider three models: T5, Chronos, and Chronos-Bolt. While T5 is an LLM, Chronos and Chronos-Bolt are TSFMs. The three models we compare have the same base size, and each model contains 12 encoder layers and 12 decoder layers. From each layer, we take out a matrix $\mathbf{W}$, which is either the query projection matrix $\mathbf{W}_Q \in \mathbb{R}^{768 \times 768}$ or the first matrix of the MLP layer $\mathbf{W}_{\mathrm{MLP}} \in \mathbb{R}^{3072 \times 768}$. We apply an SVD to the weight matrix $\mathbf{W} = \mathbf{U}\boldsymbol{\Sigma}\mathbf{V}^{\top}$ and construct a histogram out of all relative singular values in $\mathrm{diag}(\boldsymbol{\Sigma})/\boldsymbol{\Sigma}_{1,1}$.
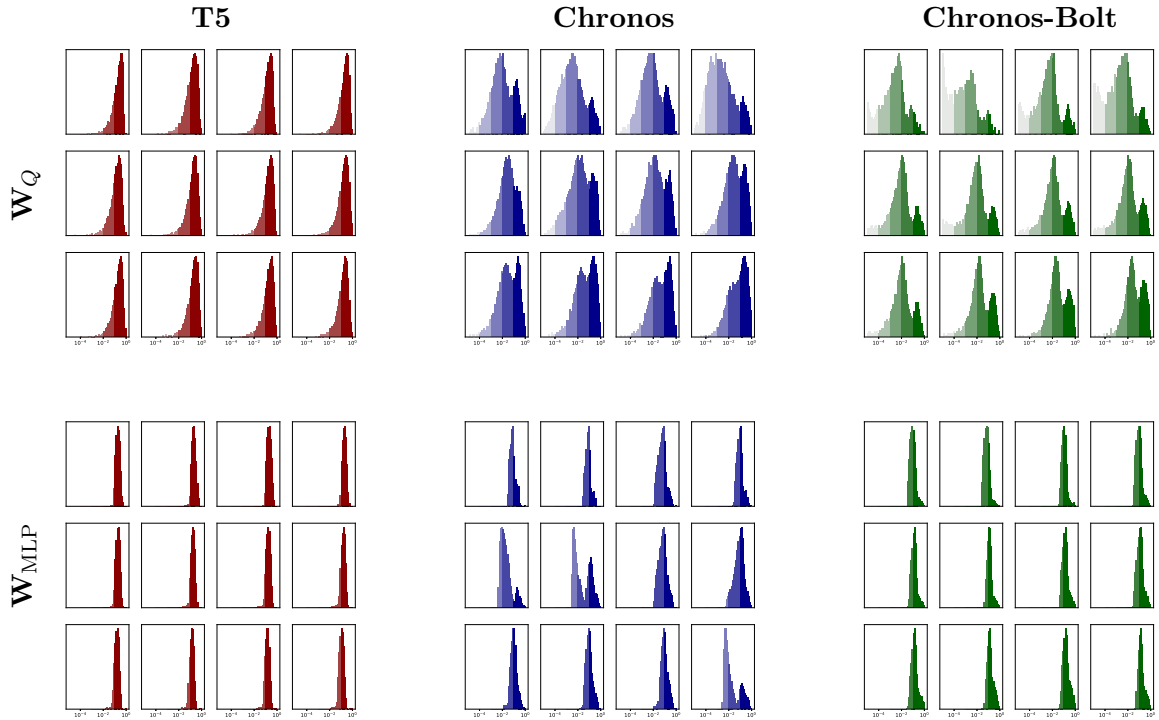

Figure 12: The distribution of all relative singular values in a weight matrix $\mathbf{W}$ in a T5, Chronos, or Chronos-Bolt model. We use five progressively fainter face colors to indicate the range where the relative singular values are in the (`1e-5`, `1e-4`], (`1e-4`, `1e-3`], (`1e-3`, `1e-2`], (`1e-2`, `1e-1`], and (`1e-1`, `1e0`] ranges, respectively. Each model contains 12 encoder layers, and we arrange the corresponding 12 weight matrices in row-major order. Note that all histograms are made on a semilog-x scale.

From Figure 12, we make some observations that align with the major claims made in the main manuscript:

1. The relative singular values decay faster for Chronos and Chronos-Bolt and they decay much slower for T5. The reason is that TSFMs leverage low-rank embeddings and do not require high-rank attention matrices, which is not the case for T5, which inevitably needs a high-rank embedding.
2. In Chronos and Chronos-Bolt, when the layers get deeper, we generally have a higher-rank structure. This aligns with the flow-of-ranks idea: as an input is pushed through more

nonlinear attention and MLP layers, its rank gets higher, and we need higher-rank attention matrices.

3. The attention matrices are generally more compressible than MLP matrices. This is not surprising, because the attention matrices in these models are square matrices, making low-rank structures much easier to emerge than in a rectangular MLP matrix.

G.2 Watching the Weights of TSFMs During Training

Another mysterious finding that we used in the main manuscript is that the attention matrices in a pretrained Chronos or Chronos-Bolt model all demonstrate low-rank structure; however, while Theorem 3 only suggests that the attention matrices *can* be written in a low-rank form, it does not preclude these matrices from having a high-rank form. To understand why the attention matrices happen to exhibit a low-rank structure, we watch the training dynamics of these attention matrices, where we pretrain a small Chronos model and record the six weight matrices in its six encoder layers at a few different training steps. Unlike Figure 12, in Figure 13, we do not show the relative singular values σ_j/σ_1. The reason will be clear later.
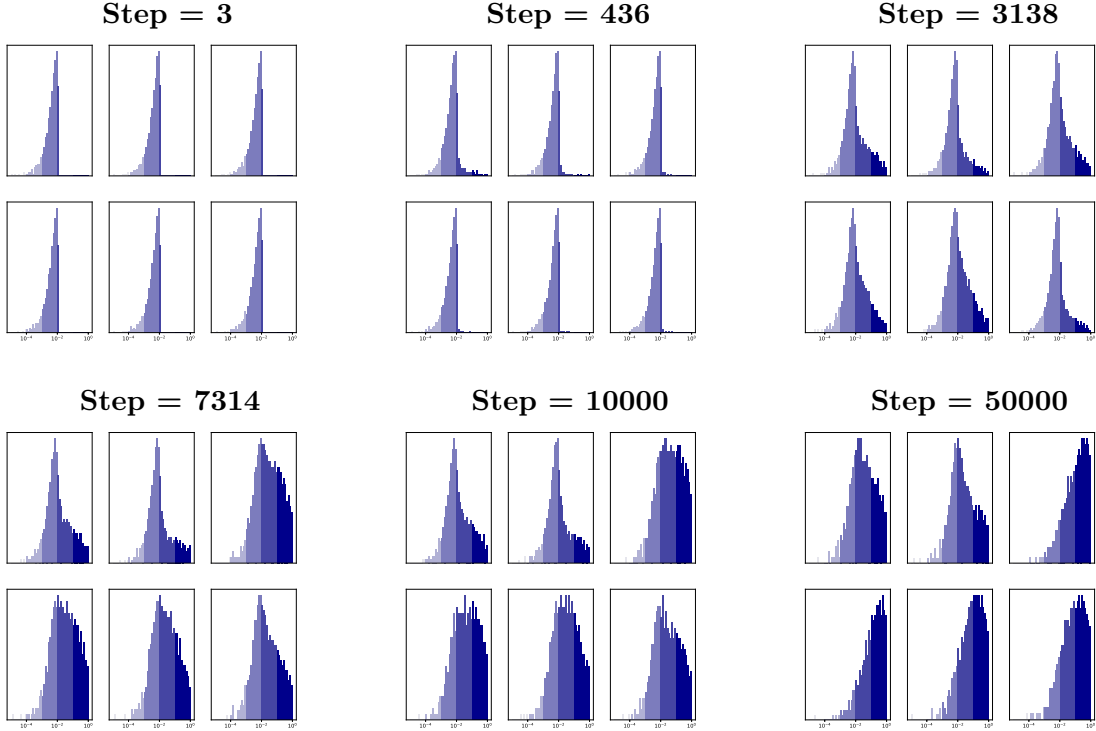

Figure 13: The distribution of all absolute singular values in a weight matrix $\mathbf{W}_Q$ in a Chronos model over training. The model contains 6 encoder layers, and we arrange the corresponding 6 weight matrices in row-major order. Note that all histograms are made on a semilog-x scale.

We note that the initialization of Chronos typically relies on a very small scaling factor. That is, the weights are all initialized to be small. From Figure 13, we see that the weight matrices are eventually learned to be larger: that is, by looking at the absolute singular values instead of the relative ones, we see that the leading singular value, i.e., the norm of the weight matrix $\mathbf{W}_Q$, eventually gets larger. When they get larger, we note that the low-rank structure evolves. This "learning the leading singular direction" interpretation is more plausible than if the weight matrix $\mathbf{W}_Q$ is initialized large, because it has no incentive to "forget the residual ranks" when it does not need to.

G.3 Watching the Weights in a Multihead Attention

In Figure 16, we showed the "correlation matrix" of a three-head attention matrix $\mathbf{W}_Q$. In Figure 14, we show more of these matrices when a different number of heads h. For each number of heads h, we can see clearly h low-rank blocks on the diagonal, corresponding to the in-head low-rank attention.
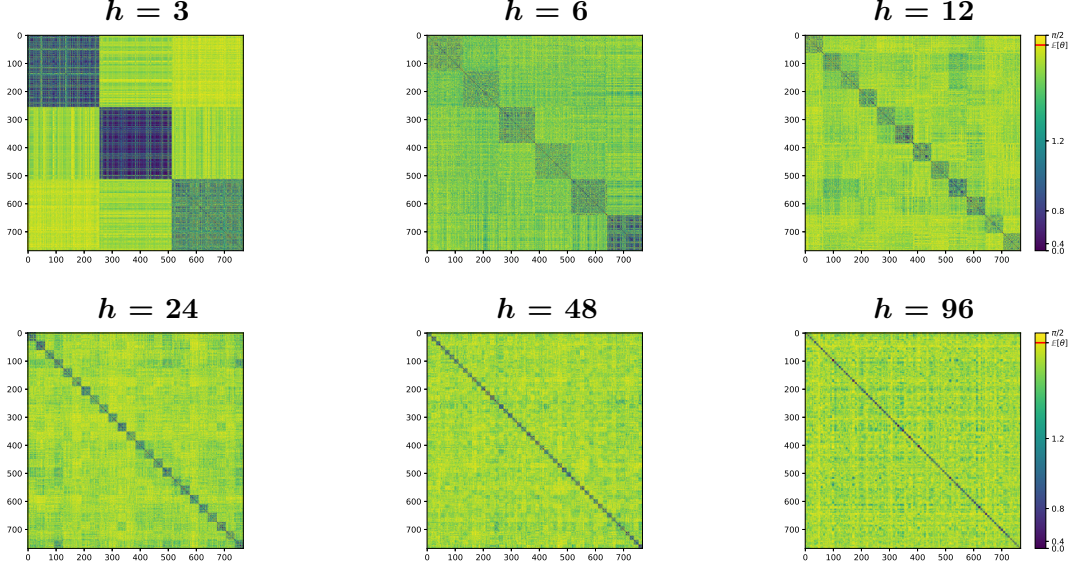

Figure 14: We pretrain a Chronos model with a different number of heads h. As h changes, we show the angle between every pair of rows of $\mathbf{W}_Q$ in the first encoder layer.

One interesting observation we can make is that the off-diagonal parts of the heatmaps, while much more yellowish than the diagonal parts, also have block structures. This is expected: if the rows in each head are very colinear, then when you compare rows between two different heads, they should share a similar angle. That is, we have a duality that not only holds for attention matrices but also holds in general: the darker a diagonal block is, the clearer the edges of off-diagonal blocks in the same row of blocks will be.

The off-diagonal parts of attention matrices, while much more orthogonal than the rows within each head, are still far from random. This means the heads themselves are also somewhat correlated, which is not surprising given that the row spaces of query, key, and value matrices are subspaces of the potentially low-dimensional row space of the input and that the models are trained with a single objective. There are two forces pulling against each other: a head-dependent random initialization, which "orthogonalizes" different heads, and a head-independent training objective that tries to align these heads.

There is a third trend (and the second duality) that is also very interesting: darker diagonal blocks seem to correspond to lighter off-diagonal blocks. There is one potential explanation for that: if the diagonal blocks are very dark, that means each head only attends to a tiny bit of information of the input. In order to obtain good results, other heads must incorporate the remaining bits of the input, resulting in very different sketchings and larger angles. On the other hand, if the diagonal blocks are brighter, that means it already contains a fair amount of information about the input, and lots of the input information is shared across heads. Hence, they should be much more correlated during training.

H More on the Chebyshev Embedding

In Figure 4, we show an experiment where we increase the rank of a fixed input embedding and watch the numerical ranks of pretrained Chronos models with that embedding. Here, we further explain how we can control the rank of this fixed input embedding function using Chebyshev polynomials. To motivate our design, we first consider how we can compute a rank-1 embedding function $\mathbf{\Phi}_1 : \mathbb{R} \to \mathbb{R}^d$. In this case, what $\mathbf{\Phi}_1$ needs to do is to map the real line linearly onto a one-dimensional subspace of $\mathbb{R}^d$. That is, we can set $\mathbf{\Phi}_1(x) = x\mathbf{u}$ for some fixed unit vector $\mathbf{u} \in \mathbb{R}^d$.
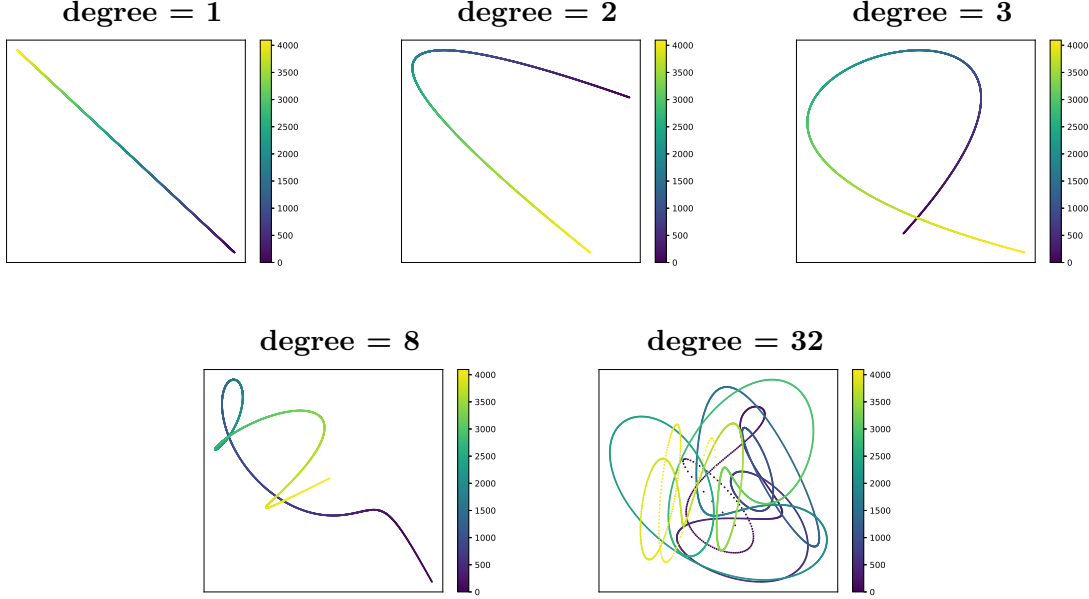

Figure 15: Visualization of the Chebyshev embeddings. For each embedding, we visualize the first two dimensions out of the 768 in the hidden space. There are 4096 points embedded in the hidden space, whose corresponding values in the input domain range from -15 to 15.

Now, how can we use this idea to design a rank-k embedding $\mathbf{\Phi}_k(x)$? One way to do that is by considering the following extension of $\mathbf{\Phi}_k$:

$$\mathbf{\Phi}_k : \mathbb{R} \to \mathbb{R}^d, \qquad x \mapsto f_1(x)\mathbf{u}_1 + \cdots + f_k(x)\mathbf{u}_k.$$

As long as the functions $f_1, \ldots, f_k$ are linearly independent, the image of the real line, $\mathbf{\Phi}_k(\mathbb{R})$, is a subset of a k-dimensional subspace of $\mathbb{R}^d$. The only question that remains is: how to choose $f_1(x), \ldots, f_k(x)$. Perhaps the easiest way to choose such a basis is by making them monomials: $f_j(x) = x^j$. However, the monomial basis often suffers from many numerical stability issues and is not ideal for the embedding, e.g., for a large j, the set $\{x, \ldots, x^j\}$ is very ill-conditioned. To choose a well-conditioned basis, we use Chebyshev polynomials, which are orthogonal on $[-1, 1]$. That is, we set $f_j(x) = T_j(x/x_{\max})$, where $x_{\max}$ is the maximum number considered in quantization, which equals 15 in the case of Chronos. Given a set of points $x_1, \ldots, x_L$ to embed, we assemble the embedded matrix $\mathbf{X} \in \mathbb{R}^{d \times L}$ as follows:

1. Sample orthonormal random column vectors $\mathbf{u}_1, \ldots, \mathbf{u}_k \in \mathbb{R}^{d \times 1}$.

2. Compute row vectors $\mathbf{f}_1, \ldots, \mathbf{f}_k \in \mathbb{R}^{1 \times L}$, where the ith entry of $\mathbf{f}_j$ is $T_j(x_i/x_{\max})$.

3. Compute the outer product $\mathbf{X} = \sum_{j=1}^{k} \mathbf{u}_j \mathbf{f}_j$.

We show the visualization of our Chebyshev embeddings in Figure 15, where as see that as we increase the rank k, the embedding becomes more "complicated."

I   Compressing a multi-head attention layer

Theorem 3 concerns the compressibility of a single-head attention layer. In practice, most TSFMs use multi-head attention instead:[2]

$$\text{MH-Attention}(\mathbf{U}; \mathbf{W}_Q, \mathbf{W}_K, \mathbf{W}_V, h) = \begin{bmatrix} \text{Attention}(\mathbf{U}; \mathbf{W}_Q^{(1)}, \mathbf{W}_K^{(1)}, \mathbf{W}_V^{(1)}) \\ \vdots \\ \text{Attention}(\mathbf{U}; \mathbf{W}_Q^{(h)}, \mathbf{W}_K^{(h)}, \mathbf{W}_V^{(h)}) \end{bmatrix},$$

$$\mathbf{W}_{Q/K/V} = \begin{bmatrix} (\mathbf{W}_{Q/K/V}^{(1)})^\top & \cdots & (\mathbf{W}_{Q/K/V}^{(h)})^\top \end{bmatrix}^\top, \quad \mathbf{W}_{Q/K/V}^{(i)} \in \mathbb{R}^{d_h \times d}, \quad d_h = d/h. \tag{19}$$

This leads to the following question: does the number of heads have an effect on the numerical ranks of the attention matrices in trained Chronos models? The answer to this is positive, but there are some important subtleties. If we look at the left panel of Figure 16, then we see that if we pretrain Chronos models with fixed hidden dimension $d = 1024$ and only increase the number of heads, the numerical rank of attention matrices increases. At first, it may seem that this happens because a multi-head attention is less compressible than a single-head one, but this is not the case. It is straightforward to show that Theorem 3 holds as well for multi-head attentions (see Theorem 5 in Appendix E). In particular, if $\boldsymbol{\Xi}$ has an algebraic rank of $\tilde{d}$, then all multi-head attention matrices can be compressed to rank-$\tilde{d}$ without affecting the output.
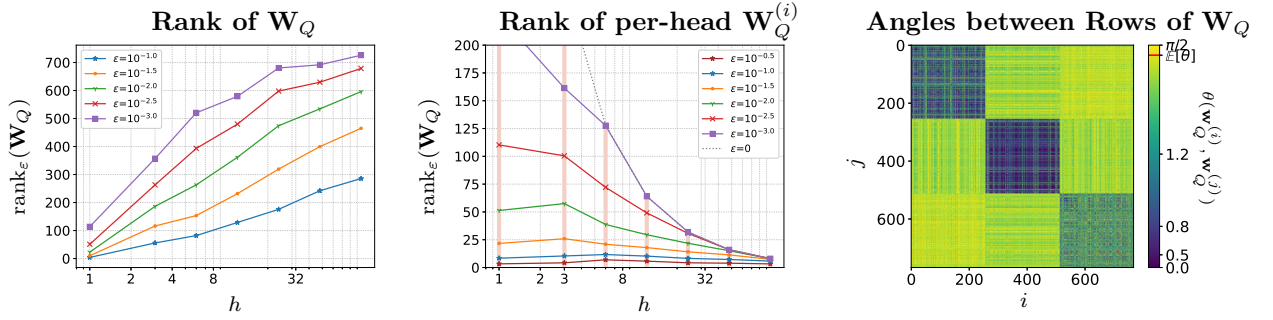

Figure 16: The left panel shows the averaged ε-rank of query projection matrices $\mathbf{W}_Q$ in pretrained Chronos models with varying number of heads. The middle panel shows the averaged ε-rank of query projection submatrices $\mathbf{W}_Q^{(i)}$ for every head. The right panel shows the angle between every pair of rows of $\mathbf{W}_Q$ in the first layer of a 3-head pretrained Chronos model.

If Theorem 5 holds for multi-head attention, then why does a multi-head attention exhibit a higher numerical rank? To understand this, we need to understand the mechanism of a low-rank weight matrix. We use $\mathbf{W}_Q$ for illustration, and the same analogous applies to $\mathbf{W}_K$ and $\mathbf{W}_V$. Let $\mathbf{W}_Q \in \mathbb{R}^{d \times d}$ be approximated by a rank-$\tilde{d}$ matrix, i.e., $\mathbf{W}_Q \approx \mathbf{W}_1 \mathbf{W}_2$, where $\mathbf{W}_1 \in \mathbb{R}^{d \times \tilde{d}}$ and $\mathbf{W}_2 \in \mathbb{R}^{\tilde{d} \times d}$. We view the action $\mathbf{W}_Q \mathbf{U}$, which maps every column of $\mathbf{U}$ from $\mathbb{R}^d$ into $\mathbb{R}^d$, as a two-step process. First, we multiply $\mathbf{W}_2$ to $\mathbf{U}$ to drop the columns of $\mathbf{U}$ from $\mathbb{R}^d$ to $\mathbb{R}^{\tilde{d}}$. In numerical linear algebra, this is known as "sketching," (Drineas & Mahoney, 2016) i.e., $\mathbf{W}_2$ "sketches" a $\tilde{d}$-dimensional subspace $R(\mathbf{W}_2 \mathbf{U})$ in $\mathbb{R}^L$, the row space of $\mathbf{W}_2 \mathbf{U}$, from a d-dimensional subspace $R(\mathbf{U})$ in $\mathbb{R}^L$.[3] If $\sigma_{\tilde{d}+1}(\mathbf{U})$ is small, then there exists a sketching matrix $\mathbf{W}_2$ so that $R(\mathbf{W}_2 \mathbf{U}) \approx R(\mathbf{U}) \supset R(\mathbf{W}_Q \mathbf{U})$; hence, we can apply a matrix $\mathbf{W}_1$ to lift the columns of $\mathbf{W}_2 \mathbf{U}$ from $\mathbb{R}^{\tilde{d}}$ back to $\mathbb{R}^d$ and have $\mathbf{W}_1 (\mathbf{W}_2 \mathbf{U}) \approx \mathbf{W}_Q \mathbf{U}$.

---

[2]In eq. (19), the $1/\sqrt{d}$ normalization factor in an attention is changed into $1/\sqrt{d_h}$.

[3]In numerical linear algebra (NLA), sketching is usually considered as an operation on the column space. To adapt it to our framework, we sketch the row space instead. This is achieved by taking the transpose of the matrix $\mathbf{U}$ and sketching its column space as usually done in NLA.

If we apply a low-rank approximation to a multi-head attention matrix $\mathbf{W}_Q$, then we obtain:

$$\begin{bmatrix} \mathbf{W}_Q^{(1)} \\ \vdots \\ \mathbf{W}_Q^{(h)} \end{bmatrix} = \mathbf{W}_Q \approx \mathbf{W}_1 \mathbf{W}_2 = \begin{bmatrix} \mathbf{W}_1^{(1)} \\ \vdots \\ \mathbf{W}_1^{(h)} \end{bmatrix} \mathbf{W}_2 = \begin{bmatrix} \mathbf{W}_1^{(1)} \mathbf{W}_2 \\ \vdots \\ \mathbf{W}_1^{(h)} \mathbf{W}_2 \end{bmatrix}, \qquad \mathbf{W}_1^{(i)} \in \mathbb{R}^{d_h \times \tilde{d}}. \qquad (20)$$

When we apply $\mathbf{W}_Q$ to $\mathbf{U}$, for each head $1 \leq i \leq h$, $\mathbf{W}_2$ sketches a $\tilde{d}$-dimensional subspace from the row space of $\mathbf{U}$ while $\mathbf{W}_1^{(i)}$ forms d_h rows from this $\tilde{d}$-dimensional space. This makes the problem clear: in an "optimal" low-rank approximation of $\mathbf{W}_Q$, the sketching matrix $\mathbf{W}_2$ is shared across all heads. Since each head is independent from the others in a multi-head attention, there is no guarantee that, in a pretrained model, the sketching matrices will be shared. In the right panel of Figure 16, we visualize the angles (see eq. (2)) between every pair of rows of $\mathbf{W}_Q$. If $\mathbf{W}_2$ is shared across all heads, then all rows of $\mathbf{W}_Q$ should exhibit some linear dependency. We only see low-rank structures within each head $\mathbf{W}_Q^{(i)}$ (i.e., the dark $d_h \times d_h$ blocks along the diagonal). This shows that instead of eq. (20), $\mathbf{W}_Q$ from a pretrained Chronos model looks more like

$$\begin{bmatrix} \mathbf{W}_Q^{(1)} \\ \vdots \\ \mathbf{W}_Q^{(h)} \end{bmatrix} = \mathbf{W}_Q \approx \begin{bmatrix} \mathbf{W}_1^{(1)} \mathbf{W}_2^{(1)} \\ \vdots \\ \mathbf{W}_1^{(h)} \mathbf{W}_2^{(h)} \end{bmatrix}, \qquad \mathbf{W}_1^{(i)} \in \mathbb{R}^{d_h \times \tilde{d}}, \qquad \mathbf{W}_2^{(i)} \in \mathbb{R}^{\tilde{d} \times d}, \qquad (21)$$

which leverages a head-dependent sketching $\mathbf{W}_2^{(i)}$. The rank of the right-hand side matrix in eq. (21), which consists of h rank-$\tilde{d}$ submatrices, can be as large as $h\tilde{d}$. This finding explains the phenomenon we observed at the beginning of this section, i.e., while the numerical rank $\tilde{d}$ of the input stays the same, the rank of the attention matrices increases with the number of heads h. The middle panel of Figure 16 confirms this numerically. We see that the numerical rank of the projection matrix $\mathbf{W}_Q^{(i)}$ in each head remains relatively constant for reasonably large ε as we increase the number of heads.

Our observation in Figure 16 is empirical and explanatory: it says in a pretrained TSFM, the attention matrices $\mathbf{W}_{Q/K/V}$ are essentially doing the head-dependent sketching (see eq. (21)). From a methodological point of view, if we train a compressed model (i.e., the one that is paramaterized by $\mathbf{W}_1$ and $\mathbf{W}_2$ instead of $\mathbf{W}_Q$) from scratch, should we adopt a parameter-efficient head-independent sketching in eq. (20) or a head-dependent one, which requires more parameters? If we know the numerical rank $\tilde{d}$ of $\boldsymbol{\Xi}$ so that $\sigma_{\tilde{d}+1}(\boldsymbol{\Xi})$ is tiny, then from an approximation theory perspective, there is little loss using eq. (20). The only problem is: we do not know $\tilde{d}$ a priori. If we choose $\tilde{d}$ small enough that $\sigma_{\tilde{d}+1}(\boldsymbol{\Xi})$ is still relatively large, then the following theorem (see Appendix I for the proof) shows the benefit of using a head-dependent sketching $\mathbf{W}_2^{(h)}$ in eq. (21).

Theorem 6. Fix some $d = h \times d_h$ for two positive integers h and d_h and $L \geq d$. Let $C \geq 1$ be any stability bound. Let $1 \geq \sigma_1 \geq \sigma_2 \geq \cdots \geq \sigma_d > 0$ be any fixed sequence. There exist an input $\mathbf{U} \in \mathbb{R}^{d \times L}$ with $\sigma_j(\mathbf{U}) = \sigma_j$ for all $1 \leq j \leq d$ and three matrices $\mathbf{W}_Q, \mathbf{W}_K, \mathbf{W}_V \in \mathbb{R}^{d \times d}$, such that the following statements hold for any $\tilde{d} < d_h$:

1. Given any rank-$\tilde{d}$ matrix $\tilde{\mathbf{W}}_V \in \mathbb{R}^{d \times d}$ with $\|\tilde{\mathbf{W}}_V\|_F \leq C\|\mathbf{W}_V\|_F$, we have

$$\left\| \text{MH-Attention}(\mathbf{U}; \mathbf{W}_Q, \mathbf{W}_K, \mathbf{W}_V, h) - \text{MH-Attention}(\mathbf{U}; \mathbf{W}_Q, \mathbf{W}_K, \tilde{\mathbf{W}}_V, h) \right\|_2 \geq \frac{1}{2}\sigma_{\tilde{d}+1}.$$

2. There exist low-rank matrices $\tilde{\mathbf{W}}_Q, \tilde{\mathbf{W}}_K, \tilde{\mathbf{W}}_V \in \mathbb{R}^{d \times d}$ with $\|\tilde{\mathbf{W}}_Q\|_F \leq \|\mathbf{W}_Q\|_F$, $\|\tilde{\mathbf{W}}_K\|_F \leq$

$\|\mathbf{W}_K\|_F$, and $\|\tilde{\mathbf{W}}_V\|_F \leq \|\mathbf{W}_V\|_F$, such that

$$\tilde{\mathbf{W}}_{Q/K/V} = \begin{bmatrix} \mathbf{W}_{Q/K/V,1}^{(1)} \mathbf{W}_{Q/K/V,2}^{(1)} \\ \hline \vdots \\ \hline \mathbf{W}_{Q/K/V,1}^{(h)} \mathbf{W}_{Q/K/V,2}^{(h)} \end{bmatrix}, \quad \mathbf{W}_{Q/K/V,1}^{(i)} \in \mathbb{R}^{d_h \times (\tilde{d}+1)}, \quad \mathbf{W}_{Q/K/V,2}^{(i)} \in \mathbb{R}^{(\tilde{d}+1) \times d},$$

where every row of $\mathbf{W}_{Q/K/V,2}^{(i)}$, except the last row of $\mathbf{W}_{K,2}^{(i)}$, contains at most d_h non-zero entries, and satisfies that

$$\left\| \text{MH-Attention}(\mathbf{U}; \mathbf{W}_Q, \mathbf{W}_K, \mathbf{W}_V, h) - \text{MH-Attention}(\mathbf{U}; \tilde{\mathbf{W}}_Q, \tilde{\mathbf{W}}_K, \tilde{\mathbf{W}}_V, h) \right\|_2 \leq 4\sqrt{h}\sigma_{h\tilde{d}+1}.$$

Theorem 6 highlights an "error-correcting" mechanism of the head-dependent low-rank design in eq. (21) in the following sense: if we choose a $\tilde{d}$ where $\sigma_{\tilde{d}+1}$ is large, then the first statement shows that the shared sketching in eq. (20) inevitably limits the expressiveness of the reduced multi-head attention layer. Using a head-dependent low-rank representation relaxes the error to the order of $\sigma_{h\tilde{d}+1}$, which can be significantly smaller than $\sigma_{\tilde{d}+1}$ when the number of heads h is large and the singular values decay fast. While using eq. (21) requires a larger number of parameters, Theorem 6 suggests the potential of a sparse parameterization of the sketching matrices $\mathbf{W}_{Q/K/V,2}^{(i)}$. We leave this as a promising future direction.

I.1 Proof of Theorem 6

We prove that a sparse but head-dependent sketching performs better in theory than a head-independent sketching, especially when $\tilde{d}$ is lower than the numerical rank of the input matrix. The intuition is that if $\tilde{d}$ is too small, then the sketching performed by a single sketching matrix must be bad, but if we use head-dependent sketchings, then we can leverage multiple of them to still obtain a lot from the input matrix.

Proof of Theorem 6. Set $\mathbf{W}_V = \mathbf{I}_d$. Interleave the singular values $\sigma_1, \ldots, \sigma_d$ as follows:

$$\boldsymbol{\sigma}^{(1)} = \left(\sigma_1^{(1)}, \sigma_2^{(1)} \ldots, \sigma_{d_h}^{(1)}\right) = \left(\sigma_1, \sigma_{h+1}, \ldots, \sigma_{(d_h-1)h+1}\right),$$

$$\boldsymbol{\sigma}^{(2)} = \left(\sigma_1^{(2)}, \sigma_2^{(2)} \ldots, \sigma_{d_h}^{(2)}\right) = \left(\sigma_2, \sigma_{h+2}, \ldots, \sigma_{(d_h-1)h+2}\right),$$

$$\vdots$$

$$\boldsymbol{\sigma}^{(h)} = \left(\sigma_1^{(h)}, \sigma_2^{(h)} \ldots, \sigma_{d_h}^{(h)}\right) = \left(\sigma_h, \sigma_{2h}, \ldots, \sigma_{d_h \cdot h}\right).$$

Define the input matrix by

$$\mathbf{U} = \left[\underbrace{\text{diag}(\text{diag}(\boldsymbol{\sigma}^{(1)}), \ldots, \text{diag}(\boldsymbol{\sigma}^{(h)}))}_{\mathbf{U}_D} \;\middle|\; \mathbf{0}_{d \times (L-d)} \right].$$

For every $1 \leq i \leq h$ and $1 \leq j \leq d_h$, let $\mathbf{v}_j^{(i)} \in \mathbb{R}^{d_h}$ be a unit vector satisfying that

$$\left\| \mathbf{v}_j^{(i)\top} \mathbf{v}_{j'}^{(i')} \right\|_2 < 1, \qquad (i,j) \neq (i',j').$$

Then, consider the following matrix:

$$\overline{\mathbf{W}}_Q = \overline{\mathbf{W}}_K = \left[\mathbf{v}_1^{(1)}/\sigma_1^{(1)} \quad \cdots \quad \mathbf{v}_{d_h}^{(1)}/\sigma_{d_h}^{(1)} \;\middle|\; \cdots \;\middle|\; \mathbf{v}_1^{(h)}/\sigma_1^{(h)} \quad \cdots \quad \mathbf{v}_{d_h}^{(h)}/\sigma_{d_h}^{(h)} \right] \in \mathbb{R}^{d_h \times d}.$$

Then, by our construction, the matrix $\mathbf{U}^\top \overline{\mathbf{W}}_Q^\top \overline{\mathbf{W}}_K \mathbf{U}$ satisfies that

$$\left(\mathbf{U}^\top \overline{\mathbf{W}}_Q^\top \overline{\mathbf{W}}_K \mathbf{U}\right)(j,j) = 1, \qquad \left|\left(\mathbf{U}^\top \overline{\mathbf{W}}_Q^\top \overline{\mathbf{W}}_K \mathbf{U}\right)(i,j)\right| < 1, \qquad i \neq j.$$

Set

$$\varepsilon = \min\left\{(1+C)^{-1}\sigma_{\tilde{d}+1}/2, \min_{1 \leq i \leq h} \sigma_{\tilde{d}+1}^{(i)} / \left(2\left\|\mathbf{W}_V \mathbf{U}\right\|_2 + 2\sigma_1\right), 1\right\}.$$

By choosing a sufficiently large $\alpha > 0$, we guarantee that

$$\left\|\underbrace{\mathrm{softmax}\left(\frac{\mathbf{U}^\top (\alpha\overline{\mathbf{W}}_Q^\top)(\alpha\overline{\mathbf{W}}_K)\mathbf{U}}{\sqrt{d_h}}\right)}_{\mathbf{G}} - \underbrace{\left[\begin{array}{c|c} \mathbf{I_d} & L^{-1}\mathbf{1}_{d\times(L-d)} \\ \hline \mathbf{0}_{(L-d)\times d} & L^{-1}\mathbf{1}_{(L-d)\times(L-d)} \end{array}\right]}_{\tilde{\mathbf{G}}}\right\|_F \leq \varepsilon. \tag{22}$$

Let query and key matrices $\mathbf{W}_Q$ and $\mathbf{W}_K$ be defined in eq. (19) using submatrices $\mathbf{W}_Q^{(i)} = \alpha\overline{\mathbf{W}}_Q$ and $\mathbf{W}_K^{(i)} = \alpha\overline{\mathbf{W}}_K$, respectively, for all $1 \leq i \leq h$. We use these matrices $\mathbf{W}_Q, \mathbf{W}_K, \mathbf{W}_V$, and $\mathbf{U}$ to prove the two claims.

Claim 1: No low-rank parameterization gets to an accuracy below $\sigma_{\tilde{d}+1}$. Let $\tilde{\mathbf{W}}_V \in \mathbb{R}^{d\times d}$ be any rank-$\tilde{d}$ matrix. We can write the approximation error as

$$\left\|\mathrm{MH\text{-}Attention}(\mathbf{U}; \mathbf{W}_Q, \mathbf{W}_K, \mathbf{W}_V, h) - \mathrm{MH\text{-}Attention}(\mathbf{U}; \mathbf{W}_Q, \mathbf{W}_K, \tilde{\mathbf{W}}_V, h)\right\|_2$$

$$= \left\|\left[\begin{array}{c} \mathbf{W}_V^{(1)}\mathbf{U}\mathbf{G} \\ \hline \vdots \\ \hline \mathbf{W}_V^{(h)}\mathbf{U}\mathbf{G} \end{array}\right] - \left[\begin{array}{c} \tilde{\mathbf{W}}_V^{(1)}\mathbf{U}\mathbf{G} \\ \hline \vdots \\ \hline \tilde{\mathbf{W}}_V^{(h)}\mathbf{U}\mathbf{G} \end{array}\right]\right\|_2$$

$$\geq \underbrace{\left\|\left[\begin{array}{c} \mathbf{W}_V^{(1)}\mathbf{U}\tilde{\mathbf{G}} \\ \hline \vdots \\ \hline \mathbf{W}_V^{(h)}\mathbf{U}\tilde{\mathbf{G}} \end{array}\right] - \left[\begin{array}{c} \tilde{\mathbf{W}}_V^{(1)}\mathbf{U}\tilde{\mathbf{G}} \\ \hline \vdots \\ \hline \tilde{\mathbf{W}}_V^{(h)}\mathbf{U}\tilde{\mathbf{G}} \end{array}\right]\right\|_2}_{E_{\mathrm{lead}}} - \underbrace{\left\|\left[\begin{array}{c} (\mathbf{W}_V^{(1)} - \tilde{\mathbf{W}}_V^{(1)})\mathbf{U}(\mathbf{G}-\tilde{\mathbf{G}}) \\ \hline \vdots \\ \hline (\mathbf{W}_V^{(h)} - \tilde{\mathbf{W}}_V^{(h)})\mathbf{U}(\mathbf{G}-\tilde{\mathbf{G}}) \end{array}\right]\right\|_2}_{E_{\mathrm{trail}}}.$$

To control E_{trail}, we note that

$$E_{\mathrm{trail}} \leq \max_{1 \leq i \leq h}\left\|(\mathbf{W}_V^{(i)} - \tilde{\mathbf{W}}_V^{(i)})\mathbf{U}(\mathbf{G}-\tilde{\mathbf{G}})\right\|_2 \leq \max_{1 \leq i \leq h}\left(\left\|\mathbf{W}_V^{(i)}\right\|_2 + \left\|\tilde{\mathbf{W}}_V^{(i)}\right\|_2\right)\left\|\mathbf{G}-\tilde{\mathbf{G}}\right\|_2 \tag{23}$$

$$\leq (1+C)\varepsilon = \frac{1}{2}\sigma_{\tilde{d}+1}.$$

To control E_{lead}, we note that

$$\left[\begin{array}{c} (\mathbf{W}_V^{(1)} - \tilde{\mathbf{W}}_V^{(1)})\mathbf{U}\tilde{\mathbf{G}} \\ \hline \vdots \\ \hline (\mathbf{W}_V^{(h)} - \tilde{\mathbf{W}}_V^{(h)})\mathbf{U}\tilde{\mathbf{G}} \end{array}\right] = \left[\begin{array}{c} (\mathbf{W}_V^{(1)} - \tilde{\mathbf{W}}_V^{(1)})\left[\begin{array}{c|c} \mathbf{U}_D & L^{-1}\mathbf{U}_D\mathbf{1}_{d\times(L-d)} \end{array}\right] \\ \hline \vdots \\ \hline (\mathbf{W}_V^{(h)} - \tilde{\mathbf{W}}_V^{(h)})\left[\begin{array}{c|c} \mathbf{U}_D & L^{-1}\mathbf{U}_D\mathbf{1}_{d\times(L-d)} \end{array}\right] \end{array}\right].$$

Hence, we have

$$E_{\mathrm{lead}} = \left\|\left[\begin{array}{c} (\mathbf{W}_V^{(1)} - \tilde{\mathbf{W}}_V^{(1)})\mathbf{U}\tilde{\mathbf{G}} \\ \hline \vdots \\ \hline (\mathbf{W}_V^{(h)} - \tilde{\mathbf{W}}_V^{(h)})\mathbf{U}\tilde{\mathbf{G}} \end{array}\right]\right\|_2 \geq \left\|\left[\begin{array}{c} (\mathbf{W}_V^{(1)} - \tilde{\mathbf{W}}_V^{(1)})\mathbf{U}_D \\ \hline \vdots \\ \hline (\mathbf{W}_V^{(h)} - \tilde{\mathbf{W}}_V^{(h)})\mathbf{U}_D \end{array}\right]\right\|_2 \tag{24}$$

$$= \left\|\mathbf{W}_V\mathbf{U}_D - \tilde{\mathbf{W}}_V\mathbf{U}_D\right\|_2 \geq \sigma_{\tilde{d}+1},$$

35

where the last inequality follows from the fact that the singular values of $\mathbf{W}_V \mathbf{U}_D$ are exactly $\sigma_1, \ldots, \sigma_d$ and $\tilde{\mathbf{W}}_V \mathbf{U}_D$ is a matrix whose rank is at most $\tilde{d}$. Combining eq. (23) and (24), we have

$$
\left\| \text{MH-Attention}(\mathbf{U}; \mathbf{W}_Q, \mathbf{W}_K, \mathbf{W}_V, h) - \text{MH-Attention}(\mathbf{U}; \mathbf{W}_Q, \mathbf{W}_K, \tilde{\mathbf{W}}_V, h) \right\|_2
$$
$$
\geq E_{\text{lead}} - E_{\text{trail}} \geq \frac{1}{2} \sigma_{\tilde{d}+1}.
$$

Claim 2: A sparse parameterization gets to an accuracy below $\sigma_{h\tilde{d}+1}$. For every $1 \leq i \leq h$, define $\mathbf{W}_{V,L}^{(i)} \in \mathbb{R}^{d_h \times \tilde{d}}$ and $\mathbf{W}_{V,R}^{(i)} \in \mathbb{R}^{\tilde{d} \times d}$ as follows:

$$
\mathbf{W}_{V,L}^{(i)} = \left[\begin{array}{c} \mathbf{I}_{\tilde{d}} \\ \mathbf{0}_{(d_h - \tilde{d}) \times \tilde{d}} \end{array} \right], \qquad \mathbf{W}_{V,R}^{(i)} = \left[\begin{array}{c|c|c} \mathbf{0}_{\tilde{d} \times d_h(i-1)} & \mathbf{I}_{\tilde{d}} & \mathbf{0}_{\tilde{d} \times ((d_h - \tilde{d}) + d_h(h-i))} \end{array} \right].
$$

Then, we have

$$
\mathbf{W}_{V,L}^{(i)} \mathbf{W}_{V,R}^{(i)} \mathbf{U} = \left[\begin{array}{c|c|c} \mathbf{0}_{\tilde{d} \times d_h(i-1)} & \text{diag}\left(\sigma_1^{(i)}, \ldots, \sigma_{\tilde{d}}^{(i)}\right) & \mathbf{0}_{\tilde{d} \times ((d_h - \tilde{d}) + d_h(h-i))} \\ \hline \mathbf{0}_{(d_h - \tilde{d}) \times d_h(i-1)} & \mathbf{0}_{(d_h - \tilde{d}) \times \tilde{d}} & \mathbf{0}_{(d_h - \tilde{d}) \times ((d_h - \tilde{d}) + d_h(h-i))} \end{array} \right],
$$

while

$$
\mathbf{W}_V^{(i)} \mathbf{U} = \left[\begin{array}{c|c|c} \mathbf{0}_{\tilde{d} \times d_h(i-1)} & \text{diag}\left(\sigma_1^{(i)}, \ldots, \sigma_{d_h}^{(i)}\right) & \mathbf{0}_{\tilde{d} \times d_h(h-i)} \end{array} \right].
$$

Hence, we have that

$$
\|\mathbf{W}_V^{(i)} \mathbf{U} - \mathbf{W}_{V,L}^{(i)} \mathbf{W}_{V,R}^{(i)} \mathbf{U}\|_2 = \sigma_{\tilde{d}+1}^{(i)}. \tag{25}
$$

Similarly, let $\mathbf{W}_{Q,L}^{(i)}, \mathbf{W}_{K,L}^{(i)} \in \mathbb{R}^{d_h \times (\tilde{d}+1)}$ and $\mathbf{W}_{Q,R}^{(i)}, \mathbf{W}_{K,R}^{(i)} \in \mathbb{R}^{(\tilde{d}+1) \times d}$ be given by

$$
\mathbf{W}_{Q,L}^{(i)} = \mathbf{W}_{K,L}^{(i)} = \alpha \left[\begin{array}{cccc} \mathbf{v}_1^{(i)}/\sigma_1^{(i)} & \cdots & \mathbf{v}_{\tilde{d}}^{(i)}/\sigma_{\tilde{d}}^{(i)} & \mathbf{v}_1^{(i')} \end{array} \right], \qquad i' = \text{mod}(i, h) + 1,
$$

$$
\mathbf{W}_{Q,R}^{(i)} = \begin{cases} \left[\begin{array}{c|c} \mathbf{I}_{\tilde{d}} & \mathbf{0}_{d-\tilde{d}} \\ \hline \mathbf{0}_{1 \times \tilde{d}} & [1/\sigma_{\tilde{d}+1}, 0, \ldots, 0] \end{array} \right], & i = 1, \\[4mm] \left[\begin{array}{c|c|c} \mathbf{0}_{\tilde{d} \times d_h(i-1)} & \mathbf{I}_{\tilde{d}} & \mathbf{0}_{\tilde{d} \times ((d_h - \tilde{d}) + d_h(h-i))} \\ \hline [1/\sigma_1, 0, \ldots, 0] & \mathbf{0}_{1 \times \tilde{d}} & \mathbf{0}_{1 \times ((d_h - \tilde{d}) + d_h(h-i))} \end{array} \right], & i > 1, \end{cases}
$$

$$
\mathbf{W}_{K,R}^{(i)} = \left[\begin{array}{c|c|c} \mathbf{0}_{\tilde{d} \times d_h(i-1)} & \mathbf{I}_{\tilde{d}} & \mathbf{0}_{\tilde{d} \times ((d_h - \tilde{d}) + d_h(h-i))} \\ \hline [1/\sigma_1, \ldots, 1/\sigma_{d_h(i-1)}] & \mathbf{0}_{1 \times \tilde{d}} & [1/\sigma_{d_h(i-1)+\tilde{d}+1}, \ldots, 1/\sigma_d] \end{array} \right].
$$

Note that since we have $\|\mathbf{v}_j^{(i)}\|_2$ for every $1 \leq i \leq h$ and $1 \leq j \leq d_h$, we clearly have that $\|\mathbf{W}_{Q,L}^{(i)} \mathbf{W}_{Q,R}^{(i)}\|_F \leq \|\alpha \overline{\mathbf{W}}_Q\|_F$ and $\|\mathbf{W}_{K,L}^{(i)} \mathbf{W}_{K,R}^{(i)}\|_F = \|\alpha \overline{\mathbf{W}}_K\|_F$ for every $1 \leq i \leq h$. Hence, we have $\|\tilde{\mathbf{W}}_Q\|_F \leq \|\mathbf{W}_Q\|_F$ and $\|\tilde{\mathbf{W}}_K\|_F = \|\mathbf{W}_K\|_F$. From now on, we only argue for the first head, i.e., $i = 1$. The rest follows easily from symmetry. Set $i = 1$, we have

$$
\left(\underbrace{\mathbf{U}^\top \mathbf{W}_{Q,R}^{(1)}{}^\top \mathbf{W}_{Q,L}^{(1)}{}^\top \mathbf{W}_{K,L}^{(1)} \mathbf{W}_{K,R}^{(1)}}_{\tilde{\mathbf{T}}^{(1)}} \mathbf{U} \right)(j,k) = \alpha^2 \begin{cases} \mathbf{v}_j^{(1)}{}^\top \mathbf{v}_k^{(1)}, & 1 \leq j \leq \tilde{d}, \quad 1 \leq k \leq \tilde{d}, \\ \mathbf{v}_j^{(1)}{}^\top \mathbf{v}_1^{(2)}, & 1 \leq j \leq \tilde{d}, \quad \tilde{d} < k \leq d, \\ \mathbf{v}_1^{(2)}{}^\top \mathbf{v}_k^{(1)}, & j = \tilde{d} + 1, \quad 1 \leq k \leq \tilde{d}, \\ \mathbf{v}_1^{(2)}{}^\top \mathbf{v}_1^{(2)}, & j = \tilde{d} + 1, \quad \tilde{d} < k \leq d, \\ 0, & \text{otherwise.} \end{cases}
$$

That is, for $1 \leq j \leq d$, the jth column of $\tilde{\mathbf{T}}^{(1)}$ has exactly one entry that equals 1, which is the jth element for $1 \leq j \leq \tilde{d}$ and the $(j+1)$st element for $j > \tilde{d}$. Moreover, for $j > d$, the jth column of $\tilde{\mathbf{T}}^{(1)}$ is zero. Hence, from the definition of α, we have

$$\left\| \text{softmax}\left(\tilde{\mathbf{T}}^{(1)}\right)(1:\tilde{d},:) - \mathbf{G}(1:\tilde{d},:) \right\|_2 \leq \left\| \text{softmax}\left(\tilde{\mathbf{T}}^{(1)}\right)(1:\tilde{d},:) - \tilde{\mathbf{G}}(1:\tilde{d},:) \right\|_2 + \left\| \tilde{\mathbf{G}} - \mathbf{G} \right\|_2 \leq 2\varepsilon. \tag{26}$$

Combine eq. (25) and (26). We have

$$\left\| \mathbf{W}_V^{(1)} \mathbf{U}\mathbf{G} - \mathbf{W}_{V,L}^{(1)} \mathbf{W}_{V,R}^{(1)} \mathbf{U} \, \text{softmax}\left(\tilde{\mathbf{T}}^{(1)}\right) \right\|_2$$

$$\leq \left\| \mathbf{W}_V^{(1)} \mathbf{U}\mathbf{G} - \mathbf{W}_{V,L}^{(1)} \mathbf{W}_{V,R}^{(1)} \mathbf{U}\mathbf{G} \right\|_2 + \left\| \mathbf{W}_{V,L}^{(1)} \mathbf{W}_{V,R}^{(1)} \mathbf{U}\mathbf{G} - \mathbf{W}_{V,L}^{(1)} \mathbf{W}_{V,R}^{(1)} \mathbf{U} \, \text{softmax}\left(\tilde{\mathbf{T}}^{(1)}\right) \right\|_2$$

$$= \left\| \mathbf{W}_V^{(1)} \mathbf{U}\mathbf{G} - \mathbf{W}_{V,L}^{(1)} \mathbf{W}_{V,R}^{(1)} \mathbf{U}\mathbf{G} \right\|_2 + \left\| \mathbf{W}_{V,L}^{(1)} \mathbf{W}_{V,R}^{(1)} \mathbf{U} \left(\mathbf{G} - \text{softmax}\left(\tilde{\mathbf{T}}^{(1)}\right) \right)(1:\tilde{d},:) \right\|_2$$

$$\leq \left\| \mathbf{W}_V^{(1)} \mathbf{U} - \mathbf{W}_{V,L}^{(1)} \mathbf{W}_{V,R}^{(1)} \mathbf{U} \right\|_2 \|\mathbf{G}\|_2 + \left(\left\| \mathbf{W}_V^{(1)} \mathbf{U} \right\|_2 + \sigma_{\tilde{d}+1}^{(1)} \right) \left\| \left(\mathbf{G} - \text{softmax}\left(\tilde{\mathbf{T}}^{(1)}\right) \right)(1:\tilde{d},:) \right\|_2$$

$$\leq \sigma_{\tilde{d}+1}^{(1)}(2 + \varepsilon) + 2\varepsilon \left\| \mathbf{W}_{V,L}^{(1)} \mathbf{W}_{V,R}^{(1)} \mathbf{U} \right\|_2 \leq 4\sigma_{\tilde{d}+1}^{(1)} \leq 4\sigma_{h\tilde{d}+1},$$

where the first inequality follows from the triangle inequality, the first equation follows from the sparsity of $\mathbf{W}_{V,R}^{(1)}$, the second inequality follows from the sub-multiplicity of the spectral norm and eq. (25), the third inequality follows from eq. (25) and eq. (26), the fifth inequality follows from the definition of ε, and the last inequality follows from the definition of $\sigma_{\tilde{d}+1}^{(1)}$. Notably, this inequality holds for every head $1 \leq i \leq h$. Hence, we have

$$\left\| \text{MH-Attention}(\mathbf{U}; \mathbf{W}_Q, \mathbf{W}_K, \mathbf{W}_V, h) - \text{MH-Attention}(\mathbf{U}; \mathbf{W}_Q, \mathbf{W}_K, \tilde{\mathbf{W}}_V, h) \right\|_2$$

$$\leq \sqrt{h} \max_{1 \leq i \leq h} \left\| \mathbf{W}_V^{(i)} \mathbf{U}\mathbf{G} - \mathbf{W}_{V,L}^{(i)} \mathbf{W}_{V,R}^{(i)} \mathbf{U} \, \text{softmax}\left(\tilde{\mathbf{T}}^{(i)}\right) \right\|_2 \leq 4\sqrt{h} \, \sigma_{h\tilde{d}+1}.$$

The proof is complete. $\qquad \square$

J   Proof of Theorem 4 and Corollary 1

In this section, we prove the idea of flow-of-ranks. The upper bound is proved via a straightforward application of singular value inequalities while the lower bound requires a careful construction.

Proof of Theorem 4. We prove the two statements separately.

The upper bound. Fix a head index $1 \leq i \leq h$ and let

$$\mathbf{Y}^{(i)} = \mathbf{W}_V^{(i)} \mathbf{U} \operatorname{softmax}\left(\mathbf{T}^{(i)}\right), \qquad \mathbf{T}^{(i)} = \frac{\mathbf{U}^\top \mathbf{W}_Q^{(i)^\top} \mathbf{W}_K^{(i)} \mathbf{U}}{\sqrt{d_h}}.$$

Then, every entry of $\mathbf{T}^{(i)}$ has a magnitude no greater than 1 because every column of $\mathbf{U}$ has a 2-norm no greater than 1 and $\|\mathbf{W}_Q^{(i)^\top} \mathbf{W}_K^{(i)}\|_2 \leq \sqrt{d_h}$. Hence, every entry of $\operatorname{softmax}(\mathbf{T}^{(i)})$ has a magnitude between $L^{-1}e^{-2}$ and $L^{-1}e^2$. This means

$$\sigma_1\left(\operatorname{softmax}\left(\mathbf{T}^{(i)}\right)\right) = \left\|\operatorname{softmax}\left(\mathbf{T}^{(i)}\right)\right\|_2 \leq \left\|\operatorname{softmax}\left(\mathbf{T}^{(i)}\right)\right\|_F \leq e^2.$$

Moreover, since $\left\|\mathbf{W}_V^{(i)}\right\|_2 \leq 1$, we have that

$$\sigma_j\left(\mathbf{Y}^{(i)}\right) \leq e^2 \sigma_j(\mathbf{U}), \qquad 1 \leq j \leq d_h.$$

Fix some $1 \leq j \leq d$ and let $j_h = \lfloor (j-1)/h \rfloor + 1$. When we concatenate $\mathbf{Y}^{(i)}$ to form $\mathbf{Y}$, using the singular value inequality that $\sigma_{i+j-1}(\mathbf{A} + \mathbf{B}) \leq \sigma_i(\mathbf{A}) + \sigma_j(\mathbf{B})$ and defining $\mathbf{Y}^{\mathcal{I}}$ to be the concatenation of $\mathbf{Y}^{(i)}$ for all $i \in \mathcal{I}$, we have

$$\sigma_j\left(\mathbf{Y}\right) \leq \sigma_{j_h}\left(\mathbf{Y}^{(h)}\right) + \sigma_{j-j_h+1}\left(\mathbf{Y}^{[h-1]}\right) \leq \sigma_{j_h}\left(\mathbf{Y}^{(h)}\right) + \sigma_{j_h}\left(\mathbf{Y}^{(h-1)}\right) + \sigma_{j-2j_h+2}\left(\mathbf{Y}^{[h-2]}\right)$$

$$\leq \cdots \leq \left(\sum_{i=2}^{h} \sigma_{j_h}\left(\mathbf{Y}^{(i)}\right)\right) + \sigma_{j-(h-1)(j_h-1)}\left(\mathbf{Y}^{(1)}\right) \leq \sum_{i=1}^{h} \sigma_{j_h}\left(\mathbf{Y}^{(i)}\right) \leq e^2 h\, \sigma_{j_h}(\mathbf{U}).$$

Hence, applying the same inequality again, we have that

$$\sigma_k(\mathbf{Z}) = \sigma_k\left(\mathbf{U} + \frac{1}{\sqrt{N}}\mathbf{Y}\right) \leq \sigma_{k-j+1}(\mathbf{U}) + \sigma_j\left(\frac{1}{\sqrt{N}}\mathbf{Y}\right) \leq \sigma_{k-j+1} + \frac{e^2 h}{\sqrt{N}} \sigma_{\lfloor (j-1)/h \rfloor + 1}. \qquad (27)$$

Moreover, from the triangle inequality, we have

$$\sigma_1(\mathbf{Z}) \geq \sigma_1(\mathbf{U}) - \sigma_1\left(\frac{1}{\sqrt{N}}\mathbf{Y}\right) \geq \sigma_1(\mathbf{U}) - \frac{1}{\sqrt{N}}e^2 h \sigma_1(\mathbf{U}) \geq \frac{1}{2}\sigma_1(\mathbf{U}). \qquad (28)$$

Combining eq. (27) and (28), we prove the theorem.

The lower bound. Let $1 = \sigma_1 \geq \cdots \geq \sigma_d > 0$ be given. Define the input matrix to be

$$\mathbf{U} = \begin{bmatrix} \operatorname{diag}(\sigma_1, \ldots, \sigma_d) & \mathbf{0}_{d \times (L-d)} \end{bmatrix}.$$

For every $1 \leq i \leq h$, let $\mathbf{W}_V^{(i)}$ be

$$\mathbf{W}_V^{(i)} = \begin{bmatrix} \mathbf{I}_{d_h - 1} & \mathbf{0}_{(d_h-1) \times (d - d_h + 1)} \\ \mathbf{0}_{1 \times (d_h - 1)} & \mathbf{0}_{1 \times (d - d_h + 1)} \end{bmatrix}.$$

Set $\varepsilon = \sqrt{N}\,\sigma_d/(5h)$. For every $1 \leq i \leq h$, let $\mathbf{P}^{(i)} \in \mathbb{R}^{L \times L}$ be the matrix so that $\mathbf{P}^{(i)}(1 : d_h, ((i-1)d_h+1) : id_h) = \mathbf{I}_{d_h}$, $\mathbf{P}^{(i)}(d_h, k) = 1$ for every $1 \leq k < (i-1)d_h$ and every $k > id_h$, and is zero elsewhere. For a sufficiently large $\alpha > 0$ determined later on, let

$$\mathbf{W}_Q^{(i)} = \alpha \left[\operatorname{diag}(\sigma_1^{-1}, \ldots, \sigma_{d_h}^{-1}) \quad \mathbf{0}_{d_h \times (d-d_h)} \right],$$

$$\mathbf{W}_K^{(i)} = \left[\begin{array}{c|c|c} \begin{array}{c} \mathbf{0}_{(d_h-1) \times (i-1)d_h} \\ \left[\sigma_1^{-1} \quad \cdots \quad \sigma_{(i-1)d_h}^{-1} \right] \end{array} & \operatorname{diag}(\sigma_{(i-1)d_h+1}^{-1}, \ldots, \sigma_{id_h}^{-1}) & \begin{array}{c} \mathbf{0}_{(d_h-1) \times (h-i)d_h} \\ \left[\sigma_{id_h+1}^{-1} \quad \cdots \quad \sigma_d^{-1} \right] \end{array} \end{array} \right].$$

Then, we have

$$\mathbf{T}^{(i)} := \mathbf{U}^\top \mathbf{W}_Q^{(i)\top} \mathbf{W}_K^{(i)} \mathbf{U}$$

$$= \alpha \left[\mathbf{I}_{d_h} \quad \mathbf{0}_{d_h \times (L-d_h)} \right]^\top \left[\begin{array}{c|c|c|c} \begin{array}{c} \mathbf{0}_{(d_h-1) \times (i-1)d_h} \\ \mathbf{1}_{1 \times (i-1)d_h} \end{array} & \mathbf{I}_{d_h} & \begin{array}{c} \mathbf{0}_{(d_h-1) \times (h-i)d_h} \\ \mathbf{1}_{1 \times (h-i)d_h} \end{array} & \mathbf{0}_{d_h \times (L-d)} \end{array} \right] = \alpha \mathbf{P}^{(i)}.$$

Therefore, by picking α sufficiently large, we have

$$\|\mathbf{G}^{(i)} - \tilde{\mathbf{G}}^{(i)}\|_2 \leq \epsilon, \quad \mathbf{G}^{(i)} := \operatorname{softmax}(\mathbf{T}^{(i)}), \quad \tilde{\mathbf{G}}^{(i)}(j,k) = \begin{cases} 1, & k = j + (i-1)d_h, \\ 1, & j = d_h \text{ and } k \leq (i-1)d_h, \\ 1, & j = d_h \text{ and } k > id_h, \\ L^{-1}, & k > d, \\ 0, & \text{otherwise.} \end{cases} \tag{29}$$

Note that we have

$$\mathbf{W}_V^{(i)} \mathbf{U} \tilde{\mathbf{G}}^{(i)} = \left[\begin{array}{ccc} \operatorname{diag}(\sigma_1, \ldots, \sigma_{h_d-1}) & 0 & \mathbf{0}_{(d_h-1) \times (L-d_h)} \\ \mathbf{0}_{1 \times (d_h-1)} & 0 & \mathbf{0}_{1 \times (L-d_h)} \end{array} \right]$$

$$\times \left[\begin{array}{c|c|c|c} \mathbf{0}_{(d_h-1) \times (i-1)d_h} & \multirow{2}{*}{$\mathbf{I}_{d_h}$} & \mathbf{0}_{(d_h-1) \times (h-i)d_h} & \multirow{2}{*}{$L^{-1}\mathbf{1}_{d_h \times (L-d)}$} \\ \mathbf{1}_{1 \times (i-1)d_h} & & \mathbf{1}_{1 \times (h-i)d_h} & \\ \hline \mathbf{0}_{(L-d_h) \times (i-1)d_h} & \mathbf{0}_{(L-d_h) \times d_h} & \mathbf{0}_{(L-d_h) \times (h-i)d_h} & L^{-1}\mathbf{1}_{(L-d_h) \times (L-d)} \end{array} \right]$$

$$= \left[\underbrace{\mathbf{0}_{d_h \times (i-1)d_h} \; \operatorname{diag}(\sigma_1, \ldots, \sigma_{h_d-1}, 0) \; \mathbf{0}_{d_h \times (h-i)d_h}}_{\mathbf{Y}_{\text{lead}}^{(i)}} \; \Bigg| \; \underbrace{\left[\begin{array}{c} L^{-1} \operatorname{diag}(\sigma_1, \ldots, \sigma_{h_d-1}) \mathbf{1}_{(d_h-1) \times (L-d)} \\ \mathbf{0}_{1 \times (L-d)} \end{array} \right]}_{\mathbf{Y}_{\text{trail}}^{(i)}} \right].$$

Note that the mulithead attention output is given by

$$\mathbf{Y} = \text{MH-Attention}(\mathbf{U}; \mathbf{W}_Q, \mathbf{W}_K, \mathbf{W}_V, h) = \left[\mathbf{Y}_{\text{lead}} \quad \mathbf{Y}_{\text{trail}} \right] + \mathbf{E},$$

$$\mathbf{Y}_{\text{lead}} = \left[\mathbf{Y}_{\text{lead}}^{(1)\top} \quad \cdots \quad \mathbf{Y}_{\text{lead}}^{(h)\top} \right]^\top, \qquad \mathbf{Y}_{\text{trail}} = \left[\mathbf{Y}_{\text{trail}}^{(1)\top} \quad \cdots \quad \mathbf{Y}_{\text{trail}}^{(h)\top} \right]^\top,$$

where

$$\|\mathbf{E}\|_2 \leq \sum_{i=1}^h \|\mathbf{W}_V^{(i)} \mathbf{U} \tilde{\mathbf{G}}^{(i)} - \mathbf{W}_V^{(i)} \mathbf{U} \tilde{\mathbf{G}}^{(i)}\|_2 \leq \sum_{i=1}^h \|\mathbf{W}_V^{(i)} \mathbf{U}\|_2 \|\mathbf{G}^{(i)} - \tilde{\mathbf{G}}^{(i)}\|_2 \leq h\varepsilon,$$

and the layer output is given by

$$\mathbf{Z} = \mathbf{U} + \frac{1}{\sqrt{N}} \mathbf{Y} = \left[\mathbf{Z}_{\text{lead}} \quad \mathbf{Z}_{\text{trail}} \right] + \frac{1}{\sqrt{N}} \mathbf{E},$$

$$\mathbf{Z}_{\text{lead}} = \operatorname{diag}(\sigma_1, \ldots, \sigma_d) + \frac{1}{\sqrt{N}} \mathbf{Y}_{\text{lead}}, \qquad \mathbf{Z}_{\text{trail}} = \frac{1}{\sqrt{N}} \mathbf{Y}_{\text{trail}}.$$

Since $\mathbf{Z}_{\text{lead}}$ is a diagonal matrix with nonnegative entries, its singular values equal its diagonal entries, which are

$$
\begin{array}{ccccc}
\sigma_1 + \frac{1}{\sqrt{N}}\sigma_1 & \sigma_2 + \frac{1}{\sqrt{N}}\sigma_2 & \cdots & \sigma_{d_h - 1} + \frac{1}{\sqrt{N}}\sigma_{d_h - 1} & \sigma_{d_h} \\
\sigma_{d_h + 1} + \frac{1}{\sqrt{N}}\sigma_1 & \sigma_{d_h + 2} + \frac{1}{\sqrt{N}}\sigma_2 & \cdots & \sigma_{d_h + (d_h - 1)} + \frac{1}{\sqrt{N}}\sigma_{d_h - 1} & \sigma_{d_h + d_h} \\
\vdots & \vdots & \ddots & \vdots & \vdots \\
\sigma_{(h-1)d_h + 1} + \frac{1}{\sqrt{N}}\sigma_1 & \sigma_{(h-1)d_h + 2} + \frac{1}{\sqrt{N}}\sigma_2 & \cdots & \sigma_{(h-1)d_h + (d_h - 1)} + \frac{1}{\sqrt{N}}\sigma_{d_h - 1} & \sigma_{(h-1)d_h + d_h}
\end{array}. \quad (30)
$$

Moreover, since $\mathbf{Z}_{\text{lead}}$ is a submatrix of $\mathbf{Z}$, the singular values of $\mathbf{Z}$ are no smaller than the singular values of $\mathbf{Z}_{\text{lead}}$. Given $1 \leq i \leq h$ and $1 \leq j \leq d_h$, let $\xi_{i,j} = \sigma_{(i-1)d_h + j} + \mathbb{1}_{\{j \neq d_h\}}\sigma_j / \sqrt{N}$ be the element in row i and column j in the array in eq. (30). Then, we have that

$$
\xi_{i,j} \leq \xi_{i',j'}, \qquad \text{for any } i \geq i' \text{ and } j \geq j'.
$$

Hence, $\xi_{i,j}$ is no greater than the $(i \times j)$th singular value of $\mathbf{Z}_{\text{lead}}$. That means for every $1 \leq i \leq h$, the kth singular value of $\mathbf{Z}_{\text{lead}}$ satisfies

$$
\sigma_k(\mathbf{Z}_{\text{lead}}) \geq \xi_{i,\lceil k/i \rceil} = \sigma_{(i-1)d_h + \lceil k/i \rceil} + \frac{\mathbb{1}_{\lceil k/i \rceil \neq d_h}}{\sqrt{N}}\sigma_{\lceil k/i \rceil}.
$$

Using Weyl's inequality, we have

$$
\sigma_k(\mathbf{Z}) \geq \sigma_k(\mathbf{Z}_{\text{lead}}) - \frac{1}{\sqrt{N}}\sigma_1(\mathbf{E}) \geq \sigma_k(\mathbf{Z}_{\text{lead}}) - \frac{h\varepsilon}{\sqrt{N}}
$$
$$
\geq \left(1 - \frac{1}{5}\right)\left(\sigma_{(i-1)d_h + \lceil k/i \rceil} + \frac{\mathbb{1}_{\lceil k/i \rceil \neq d_h}}{\sqrt{N}}\sigma_{\lceil k/i \rceil}\right).
$$

Moreover, we have

$$
\sigma_1(\mathbf{Z}) \leq \sigma_1(\mathbf{Z}_{\text{lead}}) + \sigma_1(\mathbf{Z}_{\text{trail}}) + \frac{1}{\sqrt{N}}\sigma_1(\mathbf{E}) \leq \left(1 + \frac{1}{\sqrt{N}}\right) + \frac{1}{\sqrt{N}}\|\mathbf{Y}_{\text{trail}}\|_F + \frac{1}{\sqrt{N}}h\varepsilon
$$
$$
\leq 2 + \frac{1}{\sqrt{N}}\sqrt{L \times d \times L^{-2}} + \frac{1}{5} \leq \frac{16}{5}.
$$

Combining the two inequalities above, we obtain the theorem. $\qquad\square$

The proof of Corollary 1 is a straightforward manipulation of the ceiling and floor operators.

Proof of Corollary 1. Set $j = \lfloor (hk+1)/(h+1) \rfloor$, we have

$$
\sigma_{k-j+1} = \sigma_{k - \lfloor (hk+1)/(h+1) \rfloor + 1} \leq \sigma_{\lceil k - (hk+1)/(h+1) + 1 \rceil} = \sigma_{\lceil (k+h)/(h+1) \rceil},
$$

and

$$
\sigma_{\lfloor (j-1)/h \rfloor + 1} = \sigma_{\lfloor (\lfloor (hk+1)/(h+1) \rfloor - 1)/h \rfloor + 1} \leq \sigma_{\lfloor ((hk+1)/(h+1) - 1)/h \rfloor + 1} = \sigma_{\lfloor (k+1)/(h+1) \rfloor + 1}.
$$

The corollary follows from Theorem 4. $\qquad\square$

K Additional Experiments

Pretraining a compressed Chronos. The following table supplements the figure in Figure 6.

Table 3: Results of pretraining a compressed Chronos model. We compare the performance scores *relative to the original pretrained model*. We show prediction losses for both models whose embedding matrix is randomly initialized and models whose embedding matrix is inherited from the original pretrained model. The last row is the baseline.

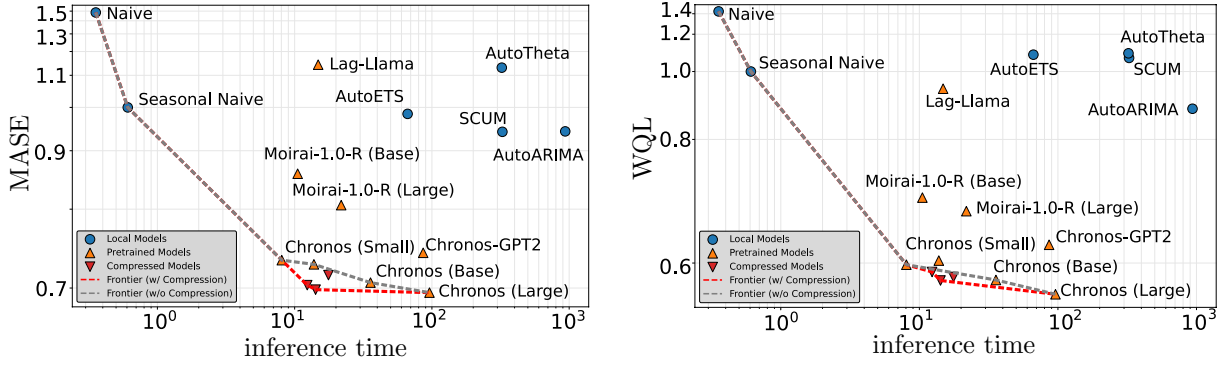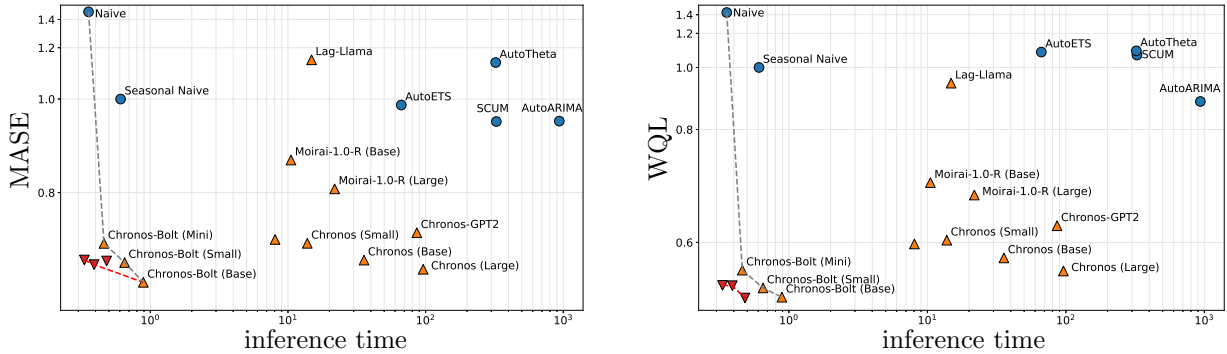| $\tilde{d}_0$	α	Size Ratio	Inference		Embedding From Scratch				Reuse Embedding			
					In-Domain		Zero-Shot		In-Domain		Zero-Shot	
			Time	Space	WQL ↓	MASE ↓	WQL ↓	MASE ↓	WQL ↓	MASE ↓	WQL ↓	MASE ↓
3	0.27	0.075	0.346	0.186	1.034	0.988	0.966	0.982	1.031	1.047	1.087	1.084
5	0.35	0.150	0.398	0.312	1.048	0.982	1.080	1.055	1.025	0.930	0.936	0.960
7	0.40	0.250	0.494	0.440	1.021	0.949	0.996	1.019	0.999	1.007	0.949	0.943
64	0.00	1.000	1.000	1.000	1.000	1.000	1.000	1.000	1.000	1.000	1.000	1.000

Table 4: Results of pretraining a compressed Chronos-Bolt (small) model. We compare the performance scores *relative to the original pretrained model*. The last row is the baseline.

$\tilde{d}_0$	α	Inference		In-Domain		Zero-Shot	
		Time	Space	WQL ↓	MASE ↓	WQL ↓	MASE ↓
2	0.25	0.517	0.802	1.005	1.004	1.013	0.999
3	0.50	0.601	0.821	1.005	0.996	1.009	1.001
5	0.70	0.740	0.840	0.980	1.003	0.991	1.010
64	0.00	1.000	1.000	1.000	1.000	1.000	1.000

Pretraining a Compressed Chronos-Bolt. In addition to Chronos, we also pretrain a compressed Chronos-Bolt model. To show the promise of compression, we start with an already-small Chronos-Bolt (small) model, based on the T5 (small) architecture. The table and figures in Table 4 can be read in the same way as those in Figure 6. In particular, we see that for both MASE and WQL, the compressed Chronos-Bolt models completely form the Pareto frontier on

our evaluation benchmark. That is, given any local method or pretrained foundation model, there exists a compressed Chronos-Bolt model that is simultaneously faster and more accurate.